PULSE ELECTRODEPOSITION OF Co-W AND ITS COMPOSITE COATINGS FOR HARD CHROME REPLACEMENTS

By

MRINALINI MULUKUTLA

Bachelor of Engineering in Metallurgical Engineering

Andhra University

VISAKHAPATNAM, ANDHRA PRADESH, INDIA

2008

Submitted to the Faculty of the
GraduateCollege of the
OklahomaStateUniversity
in partial fulfillment of
the requirements for
the Degree of
MASTER OF SCIENCE
July, 2011

PULSE ELECTRODEPOSITION OF Co-W AND ITS COMPOSITE COATINGS FOR HARD CHROME REPLACEMENTS

Thesis Approved:

Dr. Sandip P. Harimkar

Thesis Adviser

Dr. David A. Rubenstein

Dr. Kaan A. Kalkan

Dr. Mark E. Payton

Dean of the Graduate College

TABLE OF CONTENTS

Chapter Page

Chapter Page

LIST OF TABLES

Table Page

LIST OF FIGURES

Figure Page

Figure Page

CHAPTER I

INTRODUCTION

Electrolytic hard chromium coatings with high hardness/strength and wear/corrosion resistance are widely used in the industry to prevent damage to substrate materials [1]. However, the process of depositing these coatings is environmentally harmful due to disposal of toxic materials as associated wastage [2]. Various nickel- and cobalt-based alloys have been considered as replacement coatings to the electrodeposited chromium for tribological applications [7]-[8]. Among all the available alternatives, electrodeposition of tungsten with iron group metals offers a wide range of properties making them superior over other alloys. In this context, electrodeposited Co-W alloys present tremendous potential as protective and decorative coatings because of their higher hardness/sliding wear resistance and better corrosion/thermal resistance properties.

This chapter gives an overview to hard chrome plating, its significance and associated hazards. It is then followed by a briefing on the alternatives which are being currently investigated by several researchers. Electrodeposition, being a low cost, easy, and efficient method yielding good results, is chosen as the method of coating the substrate material [33]. We will then review the literature on the mechanism of pulse plating process to have a better understanding of the processing aspects of the alloys to achieve the desired properties.

1.2 Hard Chrome Plating

1.2.1 Introduction to Hard Chrome Plating

Electrodeposition of hard chrome deposits is widely recognized and being extensively used for many years in applications involving sliding or revolving parts like rotating shafts, parts of moving components like pistons, valves, rolls, compressors, etc. It enhances the life of a variety of metal parts that experience wear due to abrasion, friction, and corrosion. The low surface energy of chromium makes it more significant in such applications. This plating has very high rigidity, low coefficient of friction and high corrosion resistance making it prominent in many applications for enhancing the life of components [1]. The main advantage of this process is that it is relatively low temperature process and hence can be used to impart hard surface to any component without actually deforming it. These electrolytic coatings with high hardness/strength and wear/corrosion resistance are widely used in the industry to prevent damage to substrate materials. However, the process of depositing these coatings is environmentally harmful due to disposal of toxic materials as associated wastage [2]. Fig. 1.1 gives a few sources of hexavalent chromium originating from the plating bath and reaching the workers and environment.

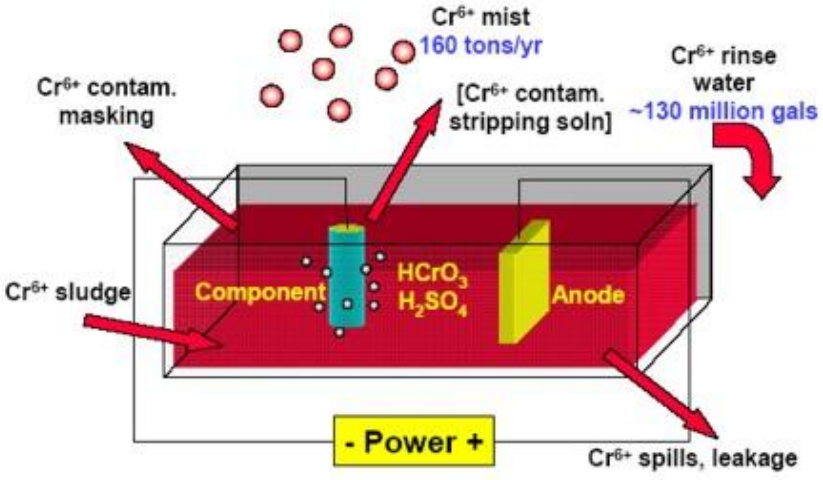

Fig. 1.1 *Sources of hexavalent chromium in the plating bath resulting in pollution and hazards[2].*

In addition to these hazards, it has other disadvantages like the formation of microcracks in the plating layers, decrease in rigidity with increase in temperature of the surroundings, low deposition rates, complexity of plating, etc. Owing to all these problems, there has been increased momentum towards finding environmentally accepted alternatives to hard chromium coatings in the recent years [6]. A number of electrodeposited alloys are of interest due to various properties like low internal stresses, magnetic properties, hardness, malleability, ductility and resistance to corrosion [7]. Electrodeposition is chosen as it is one of the most common, relatively simple, and economical coating technologies capable of depositing metal and alloy coatings with improved surface properties and microstructures [8].

1.2.2 Properties and Applications of Hard Chrome Plating

Properties of Hard Chromium

Elemental Chromium is a hard and brittle metal with high lustre, greyish-white appearance and has a high melting point of 1850 °C. Electroplated chromium can withstand heat up to 400 °C and has a lustrous appearance. Properties of chrome plating vary with a number of factors including plating parameters, testing environment, and components of electrolytic bath [1]. A range of values of hard chromium plating properties which make them attractive for numerous applications are in table 1.1.

Table 1.1 Typical properties of hard chromium deposits [1].

Property	**Value for electroplated Cr**
Hardness, as plated	450 – 1000 VPN
Hardness, on heating	
400 °C	450 – 800 VPN
600 °C	420 – 500 VPN
800 °C	250 VPN
Coefficient of linear expansion	8.1×10^{-6} $(°C)^{-1}$
Density	6.9 – 7.2 g/cm^3
Static coefficient of friction	0.17 (on steel)
Sliding coefficient of friction	0.16 (on steel)
Resistance to corrosion	Resists attack by almost all organic and inorganic compounds, except muriatic and sulphuric acids
Resistance to heat	Resistant to changes in temperature until 400 °C
Paramagnetic properties	It is paramagnetic and hence can be used to make the surface non-magnetic

These properties make the underlying industrial component perform satisfactorily under conditions like high temperature, impact forces, grinding, etc.

Industrial Applications

The application of chrome plating to components in various industries has increased rapidly over the years. It is of two types depending on the application for which the plating is being used,

namely protection of various parts from harsh environments and decorative purposes. Table 1.2 gives a list of applications of chrome plating in specific industries.

Table 1.2 Few applications of chrome plating in various industries [1].

Industry	**Applications**
Mechanical	Drills, cutters, turning tools, lathe spindles, mandrels, mounting jigs, files, bearings
Chemical	Anticorrosive coatings, hydraulic rams, plates, sheaths, tablet punches, glass moulds
Electrical	Non-magnetic parts, turbine blades, contacts
Metal	Dies, spinning tools, tube rolls, punches
Plastics	Plastic moulds, hoppers, cylinders, nozzles, mixer arms, spreaders
Fluid Power	Valves, rams, cylinder cranks, shafts
Agriculture	Spades, garden shears. hoes, plough shares
Aircraft	Crankshafts, rams, gun barrels, camshafts
Railways	Locomotive slides, dampers, cams, joints for brakes, shafts, buffer pistons
Textiles	Bobbins, protective coatings, tension parts, thread guides, printing cylinders

1.2.3 Environmental and Health Hazards

Hard chrome plating consists of hexavalent chromium in the deposit that is more dangerous and carcinogenic when compared to trivalent chromium (which occurs in nature usually); trivalent chromium is an essential trace element in the body for human metabolism. There are several

issues with the plating process and the bath used imposing severe risks on both the environment as well as the personnel. Hard chrome plating uses chromic acid solution which is responsible for the release of chromium (hexavalent) ions that are hazardous even in minor quantities [2]. These ions cause problems on exposure and when inhaled. Some of the problems relating to risks imposed on human health and environment are detailed below.

Health Effects

Inhalation and contact with skin is the primary source of exposure for workers who happen to be the worst victims of adverse effects. Short term effects include skin irritation, sneezing, headache, and ulcers in the nasal septum [3]-[4][5]. It can also cause respiratory problems, cancer in kidneys, lungs, etc when inhaled in large quantities [4].

Environmental Effects

These ions enter into environment in the form of chromate and dichromate anions from the industrial wastes, thus, contaminating air, water and soil to a considerable extent [5]-[6]. These risks are not limited to humans (or workers); they also affect the mammals, plants and marine life.

Taking all these factors into consideration, several federal regulations have been imposed by the Environmental Protection Agency (EPA) and Occupational Safety and Health Administration (OSHA) on specific industries to protect against the adverse effects by restricting the levels of exposure [6]. Also, several acts have been formulated by the government, namely, the clean air act, the clean water act, the resource conservation recovery act, and the emergency planning & community right-to-know act to determine the measures to reduce and control the levels of pollution [6]. These measures have increased the complexity of plating and also the costs of waste disposal increasing the process costs.

All the above stated factors contributed to the development of environmentally acceptable alternatives for hard chrome plating. Progress has been made by several researchers to introduce an alternative by several methods including thermal spray, weld facing, heat treatment, vapor deposition and electrodeposition [8]. Electrodeposition has proved to be a better deal for hard chrome plating when compared to all the above processes resulting in enhanced properties, also satisfying economic consideration.

1.3 Current Alternatives

There has been significant progress in the development of replacement to chrome plating resulting in a number of potential alternatives to the same. Several technologies like HVOF, plasma spraying, electrodeposition, laser cladding, plasma nitriding, electro-spark deposition, etc have been investigated with a view to develop a coating which matches the chromium in its performance and also addresses the safety concerns [6]. A list of technologies and the corresponding alternative coatings is given in Fig. 1.2. Among the listed technologies, electrodeposition is gaining lot of importance as the process meets all the general, technical requirements and is economical. HVOF, plasma and laser processes also produce coatings with excellent properties, but they have limitations relating to the size of the component to be coated, post processing of the coated parts (machining is required due to the surface roughness), availability of the equipment and complexity of the process involved. In general, electroplated coatings possess better properties than the chromium ones and hence, can be used in many applications directly.

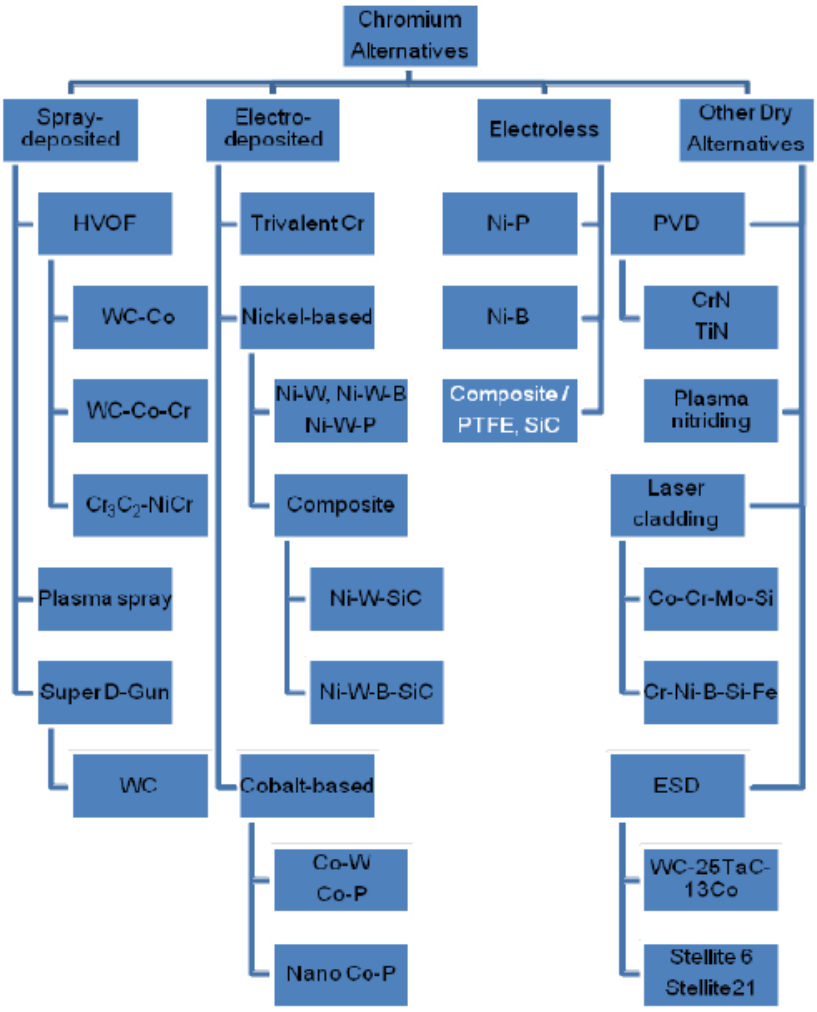

Fig. 1.2 *Current alternatives for chromium plating [6].*

Alloy and composite plating can be made to possess superior properties, especially hardness, wear, abrasion and corrosion resistance, in comparison to that of metal plating. Several alloys have been deposited and investigated for the desired properties, to produce an environmentally acceptable alternative for hard chrome plating. Fig. 1.3 shows superior hardness of few electrodeposited alloys which are being investigated demonstrating the effectiveness of the technique in producing deposits with enhanced properties.

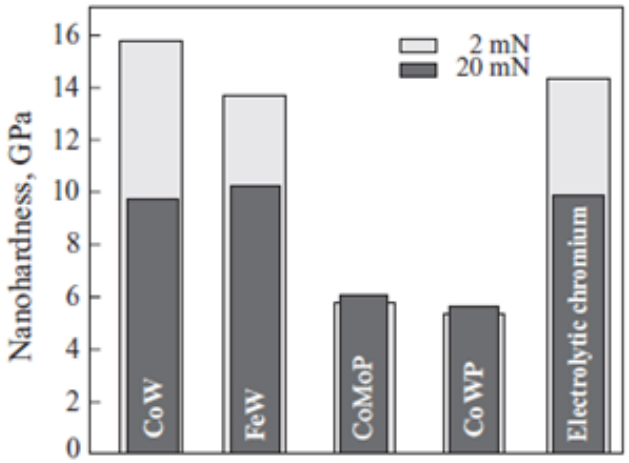

Fig. 1.3 *Nanohardness of alloys [79].*

Composite deposits consist of tiny secondary phase particles embedded in a metal or alloy matrix, thus strengthening it and improving the physical, thermal and mechanical properties. These secondary phase particles influence the overall properties and performance of the resultant deposit. Thus, composite plating can be used to develop a deposit having excellent properties and serves as an environmentally acceptable substitute to hard chrome plating.

1.3.1 Binary Alloy Electrodeposition

Co-P

Nanocrystalline cobalt-phosphorus (Co-P) coatings are obtained by electrodeposition using cobalt anode and an aqueous bath. The coatings deposited by this method have better properties including improved corrosion resistance, sliding wear resistance, hardness and tensile strength due to the controlled grain size making them comparable to hard chrome plating [9]. Deposition of nanocrystalline Co-P coatings is done by an aqueous method, making it more suitable for many applications (involving dense chrome plating) like cylinders, bevel gears, and turbine shafts. This

process eliminates worker safety concerns and environmental concerns. It also eliminates the problems because of hydrogen embrittlement yielding coatings with longer life and better performance. The main disadvantage of these coatings is that their abrasive wear behavior is lesser than the hard chrome ones. Also, hardness of these coatings depends on the phosphorus content in the coating which in turn affects the strain tolerance of the same. The nanocrystalline Co-P coatings have successfully addressed the sliding wear and corrosion aspects of the hard chrome plating making them suitable for the few applications detailed before.

Ni-W

Electrodeposited amorphous nickel-tungsten coatings, having more than 44% W are found to possess superior properties making them one other potential alternative for hard chrome plating. These amorphous coatings are found to possess a high melting point (which makes them more stable and heat resistant), high rigidity, abrasion resistance, and erosion resistance [1]-[12]. Furthermore, it is a cost effective process, and is human and environmentally friendly. Several applications like rotating cylinders, shafts, drilling equipment, and other parts in the oil and gas industry can use these coatings. The major concern for these coatings is the risk of occurrence of hydrogen embrittlement which affects the coating performance (during their service) adversely. Also, the characteristics of the coating change with the nature of the substrate and hence the substrate has to be preplated with nickel increasing the processing costs.

Co-W

Recently, Co-W alloys are attracting significant attention due to their high hardness and wear/corrosion resistance. Several researchers have successfully demonstrated PED of Co-W coatings using citrate electrolyte. These coatings, owing to their eco-friendly processing and high hardness/wear resistance, are promising for electrolytic chromium replacement. Most of these alloys are characterized by hardness ranging from 500 to 700 kg/mm^2 which is lower than that of

hard Cr coatings - chrome plating usually exhibits a hardness of ~ 900 kg/mm^2 [73]. These coatings are promising as they are deposited with good corrosion, wear properties and with very low cracking on a wide variety of substrates [57-70]. They possess good wear properties in both dry and lubricating conditions. Hence, these coatings find potential applications in many industries including aircraft, automobile and hydraulics.

1.3.2 Multi-alloy Electrodeposition

Ni-W-B

Amorphous alloys of Ni-W or Ni-W-B have gained significant attention due to their excellent erode-resistant ability and high rigidity [14]-[16]. Ni-W-B alloys have superior properties in comparison to Ni-W alloys. The addition of B reduces the micro-crack formation and improves the oxidation resistance of the alloy coating. Though this alloy is plated using the conventional plating equipment, it is more complex and costlier than chrome plating. The coatings are annealed in order to improve the hardness that is essential for wear resistant applications. The heat treatment employed influences the properties of the coating, especially the rigidity and the erosion resistance. Hardness of the coatings decreases above 400°C with increase in heat treatment temperature. At such higher temperatures, the grain size increases resulting in decreased hardness of the deposit. These ternary alloys have the surface finish and wear properties similar to that of chromium plating [15]. Also, they are comparable to chromium plating in their throwing power, reflectivity and uniformity, making them suitable for decorative applications.

Ni-Co-Fe

Nickel-iron-cobalt ternary alloys are one of the closest alternatives to hard chromium plating. They possess wear resistance which is twice that of chromium plating and corrosion resistance which is more than twice that of the same [14][12][13]-[14]. On regulating the iron and nickel contents in the deposit, similar appearance can be obtained along with the increased hardness and stability[19]. A major disadvantage of this alloy deposit is that cracks originate in these coatings easily. Though the performance of these coatings is very close to hard chrome plating, they are relatively softer, and consequently are not seen as efficient alternatives for the same.

Co-W-Fe

This ternary combination is of particular interest as codeposition of tungsten or alloys of tungsten with any of the elements of iron group gives a wide range of alloy systems that can be considered as potential hard chrome replacements. This technique of tungsten alloy plating offers a wide variety of advantages, including higher cathode current efficiency, improved throwing power, covering power, deposition of adherent deposits with moderate current densities, and neutrality of the electrolytic solution [17]-[18]. These systems exhibit high corrosion resistance, enhanced tribological and mechanical properties making them attractive among the available alternatives. However, the wear resistance of these deposits is lower than that of chromium and should be improved.

1.3.3 Composite Electrodeposition

Ni-W-SiC

Among different nanoparticulates which are used for reinforcement, SiC particles are extensively studied for their excellent hardness, high oxidation resistance, and their chemical and thermal

stability. The codeposition of SiC particles into the Ni-W matrix results in the formation of Ni-W-SiC composite coating with better properties than the Ni-W matrix. The SiC particles dispersed in the matrix strengthen it leading to an increase in the hardness and wear resistance of the resultant composite deposit. The dispersion of the SiC particles and hence the properties of the composite coating are affected by the concentration of SiC particles, current density and stirring rate of the electrolytic bath. The effect of heat treatment and SiC content on the mechanical, tribological and corrosion properties of the composite are being investigated [21-30]. Hardness and wear resistance of the composite deposits are doubled to that of chromium plating that are found to increase further on heat treatment. All these factors contributed for the overall competence of these coatings among the available alternatives.

Ni-Co-YZA

Ni-Co alloys are economical and have good thermal, physical and mechanical properties in comparison to the nickel coatings. In the recent years, YZA coatings are being extensively studied for finding applications in varied fields owing to its high temperature properties. The nano particulates are reinforced in the Ni-Co matrix by electrodeposition resulting in a significant improvement in the high temperature properties of the composite deposit obtained. The resulting composite is found to possess better mechanical, tribological, corrosion properties in addition to their thermal and chemical stability [19]. By varying the relative proportions of cobalt and YZA, the composite coating can be tailored for numerous applications. Generally, this type of composite plating is best suitable in cases where moderate corrosion resistance and high wear resistance is required.

Co-P-SiC

Cobalt base alloy coatings are being extensively studied for hard chrome replacements as they are recognized by the Environmental Protection Agency (EPA) for the reduction in the levels of

pollution caused. In this respect, Co-P-SiC coatings are investigated and found to possess good metallurgical bonding without any cracks (characteristic of hard chrome) and high ductility [7]-[9]. These are found to possess excellent fatigue and corrosion properties compared to chrome plating rendering them suitable for applications like hydraulic cylicnders, aerospace components, etc. The main disadvantage of these composite coatings is that they are not suitable for high temperature applications involving high stresses. This is due to the high phosphorus content in the coating limiting its high temperature applications beyond 400°C.

1.4 OBJECTIVE

The present study aims at finding a replacement for current hard chrome coatings that exhibits enhanced material performance and eliminates the need for the toxic and hazardous chromium electroplating baths. Efforts are directed towards electrodeposition of an amorphous alloy/composite coating that would allow for the retention of advantages of chromium plating technology. Research is carried out on the pulsed electrodeposition of Co-W and its composite coatings for the same. The objectives of this study are as follows:

- Synthesis of Co-W alloy coatings by pulsed electrodeposition
- Study of the effect of pulse electrodeposition parameters, namely, pulse on-time, pulse off-time, and pulse frequency on the properties of Co-W alloy deposits for optimization of parameters of the deposition process
- Fabrication of composite coating by reinforcing nano alumina particles into the Co-W alloy matrix in order to improve the hardness, wear and corrosion resistance of the coating
- Effect of current density on the reinforcement of Al_2O_3 in Co-W alloy matrix and properties of the resulting composites

CHAPTER II

REVIEW OF LITERATURE

2.1 Electrodeposition – Concepts and Mechanism involved

2.1.1 Electrodeposition – Introduction

Electrodeposition is one of the most common, relatively simple, and economical coating technologies capable of depositing metal and alloy coatings with improved surface properties and microstructures. A number of electrodeposited alloys are of interest due to various properties like low internal stresses, magnetic properties, hardness, malleability, ductility and resistance to corrosion [33][32]-[33]. The mechanical properties of electrodeposited alloy coatings can be further improved by composite designing (co-deposition) and microstructure improvements (formation of amorphous or nanocrystalline grain structure). The underlying mechanisms of these approaches are briefly discussed in the following sections.

2.1.2 Significance of Amorphous Alloys

Amorphous alloys stand as a separate class of materials, varying from the conventional nano and polycrystalline materials, and offering a wide variety of advantages and greater scope of applications in various industries. In spite of possessing the same composition, the crystalline and amorphous films differ considerably in their physical, mechanical and electrical properties.

A characteristic feature of amorphous materials which differentiates them from crystalline ones is that they do not have grain boundaries. There are a number of advantages of amorphous materials over crystalline ones as listed below:

1. Choice of a wide variety of alloy compositions is possible in the case of amorphous alloys. The formation of single phases restricts this possibility in case of crystalline ones.
2. The absence of grain boundaries leads to the improved corrosion and wear resistance, and better magnetic properties. Thus, amorphous alloys have better tribological properties in comparison to crystalline ones.
3. Few amorphous alloys are ductile, increasing the possibility of application of these alloys.
4. Most of them possess temperature-independent resistivity and low thermal conductivity because of their large atomic disorder.

The above mentioned advantages have led to numerous technological applications of these alloys including magneto-optical recording, corrosion-resistant coatings, transformer materials, etc. Apart from these, the metastable character of amorphous alloys is a disadvantage as they might tend to transform into the corresponding crystalline phases on variation of temperature and over a period of time.

2.1.3 Theory/Mechanism of Alloy Plating

Many kinds of amorphous alloys can be easily formed by the electrodeposition method. There are numerous reports of the work conducted using this method for decades; most of them reported an amorphous structure of the film deposited. An attempt to explain the formation mechanism of the amorphous alloys has been made by T.Watanabe, *et al [53]*[40], [53]. He described the film formation to take place in a series of steps described below. Fig. 2.1 gives a schematic diagram of the process detailed by him.

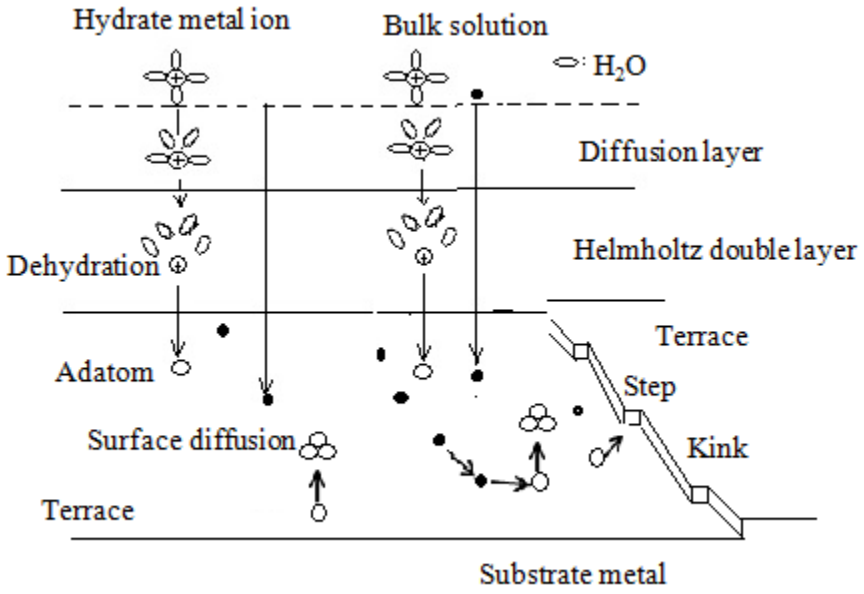

Fig. 2.1 *Schematic diagram showing different stages of formation of amorphous alloy film by electrodeposition [53].*

Metals form ions when in a solution, on application of current and potential, either become hydrated or form complexes. These ions are attracted to the cathode when a potential is applied across the electrodes and also the dipoles of water present in the diffusion layer become oriented. The ions are then dehydrated in the Helmholtz double layer and are discharged on the electrode. The discharged ions can be termed as adatoms and they are neutral atoms which diffuse on the surface of the electrode, making themselves stable at an appropriate position. The neutral atoms which are successfully precipitated on the surface of the electrode become cohesive to form nuclei and then island crystals. These island crystals grow and cover the entire cathode surface by coupling with each other. Thus, any thin film formation takes place by the process of nucleus formation and growth. The morphology of the film might change with the plating time and thickness of the film deposited. There is a possibility for appearance of kinks and steps on the coating, resulting in dendrite crystal formation which is undesirable and hence calls on for grain

refinement. Refinement of crystal grains has been made possible by several methods like use of additives or changing the plating conditions, including pH, temperature, current density, complexing agent, potential, pulse, etc. As a result of the variation of the above mentioned conditions for refinement of crystal structure, the plating films often assumed an amorphous structure.

Also, there is one more important factor which makes the film amorphous or crystalline namely the nature of the two kinds of precipitating atoms at the surface of the substrate. If the two atoms are of a similar kind, the affinity between them is greater leading to a more periodic structure of the binary alloy film formed which makes the coating crystalline. If the two atoms are of different kinds having different crystal structures, the atoms cannot have a periodical structure but assume a random structure resulting in the amorphous nature of the coating. It is also known that the energy of formation of amorphous structure is lower than that of crystalline structure, hence favoring amorphous over crystalline ones. From this, it can be inferred that the plating film will be mostly amorphous.

Thus, the mechanism of formation of amorphous alloy films can be explained. It can be concluded that all amorphous materials formed by the method stable at room temperature are alloys. An important contribution can be made to the formation of amorphous materials by making them alloys using the electrodeposition process.

2.1.4 Co-deposition Process

Composite coatings reinforced with micro- or nano-sized hard particles can be electrodeposited from a conventional electrolyte bath with suspended particles in it. The process of electrodepositing composite coatings is known as co-deposition. In general, the reinforcement of hard particles increases the hardness and strength of the composite coatings. The reinforcement of hard particles often inhibit the growth of matrix grains during the electrodeposition process

resulting in further strengthening effects. Several reviews have been published on the mechanism behind the composite plating which involves the reinforcement of solid particles such as Al_2O_3, SiC, TiO_2, and many other powders depending on the properties of the desired coating [45]-[46][47]. Several properties like hardness, strength, electrical conductivity, wear resistance and corrosion resistance of the coating can be enhanced by reinforcement of such solid and inert particles into the metal/alloy matrix [26]-[27]. The codepostion of these inert particles with metals is being investigated for the effect of parameters such as particle concentration, type, size, shape, bath constituents, temperature, pH, additives and existing models of deposition by many researchers [29][41][47].

2.1.5 Theory/Mechanism of Co-deposition Process

Most of the theoretical models have focused on the mechanisms of deposition and predicting the amount of particle incorporation in the coatings [46]-[53]. One of the earliest models to describe the codeposition process was proposed by Guglielmi *et.al* in 1972 [48]. The model describes electrophoretic attraction as the driving force behind the entrapment of particulates in the growing film. The mechanism was described in two adsorption steps: a) a loose adsorption which is physical in nature; and b) a strong adsorption that takes into account the electrochemical nature of the process. The first step of loose physical adsorption was described by a Langmuir isotherm similar to the approach of adsorption ions. The surface coverage of the particles is a function of their concentration in solution. The second step of strong adsorption was described using a Tafel kinetic expression which also included a term to account for the loose adsorption. In the second step, the particles are irreversibly adsorbed.

The volume fraction of the deposited metal was described by Faraday's law and a kinetic expression for current. His model predicts a rise in the particle concentration in the deposit with a rise in the concentration in the electrolyte. This model had been verified for the deposition of

TiO_2 and SiC from a Ni-sulfamate electrolyte. An important assumption here was that all the predictions based on this model were for the deposition on electrodes where sufficient mixing is provided and therefore mass transport and convective flows are not accounted for. This is a drawback of the model as it cannot account for deposition onto rotating cylinder electrodes where mass transport effects are dominant.

Kariapper *et al*. has also done similar adsorption studies on composite coatings [49]. They explained that the particles could be incorporated into the metal/alloy matrix if they would acquire a positive surface charge and this happens due to electrostatic attraction. They demonstrated the deposition of alumina, titania and silicon carbide of a few microns size, along with nickel from sulfamate and sulfate electrolytes.

An improvement over the Guglielmi's model was proposed by Celis *et al*. based on a statistical approach [50]-[51]. They postulated the whole process as a five-step adsorption process described as follows:

a) Initially, an adsorbed double layer of cations is formed around each particle in the bulk of the solution,

b) the particles are transferred from the bulk convection to the boundary layer,

c) these particles then diffuse through the boundary layer and reach the surface of the cathode,

d) the adsorbed electroactive cations are reduced at the cathode, and

e) the solid particles are captured by the growing film when a fraction of the adsorbed ions are reduced.

This five step process is schematically represented as shown in Fig 2.2.

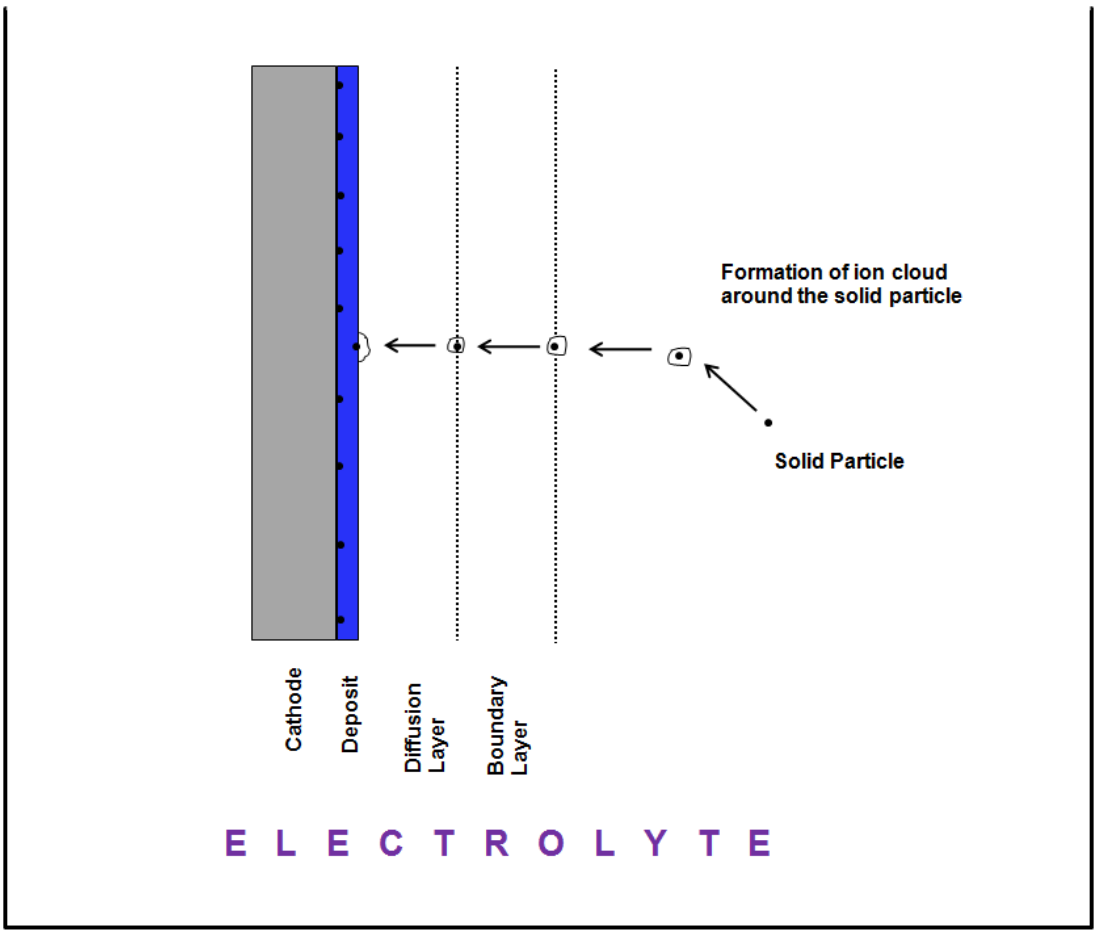

Fig. 2.2 *Schematic diagram shwing the process of codeposition and incorporation of solid particles into the deposit.*

Their model predicts the volume fraction of codeposited particles depending on the probability of a particle crossing the diffusion layer to become incorporated, the number of particles reaching the cathode and the weight of the particle. They proposed the probability of a particle being deposited at a given current in terms of a binomial distribution involving the bulk concentration, diffusion coefficient of the metal and the boundary layer thickness. The model has been verified for the codeposition of alumina with copper from an acid copper sulfate bath.

Apart from the models discussed earlier, few researchers have also attempted to explain theoretically the mechanics of the codeposition by accounting for the electrochemical and hydrodynamic forces acting on particles [45][52].

2.2 Different Electrodeposition Tehcniques

2.2.1 Direct Current Electrodeposition

In direct current plating, electrodeposition is performed in a plating unit which is connected to a DC current source. It consists of a complete circuit wherein electrons are directed from power supply to the cathode. In this kind of process, only one parameter i.e., current density can be varied. Fig. 2.3 shows typical waveform of DC electrodeposition. Duty cycle is the ratio of current ON time to total time, which is 100% in DC electrodeposition. Therefore, the average current density (Avg. current density equals to duty cycle X Peak current density) equals to the peak current density.

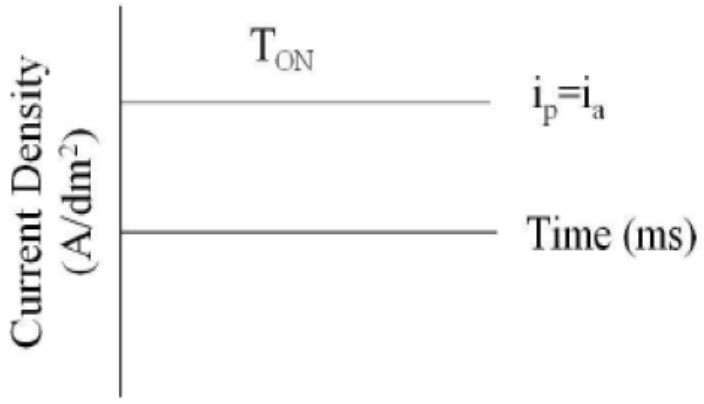

Fig. 2.3 *Schematic of direct current waveform.*

2.2.2 Pulsed Electrodeposition

In pulsed current deposition, current is imposed in a periodic manner with a rectangular form which is a powerful means of controlling the electrocrystallization process (massive nucleation and reduced grain growth) and producing deposits with unique composition and microstructure. Electrolysis is carried out at a higher current density during a short period of time (μs) using pulse electrodeposition, by which it enhances the plating rate and gives highly conducting, non-porous and finer grain deposits [34][38]. Fig. 2.4 shows shows typical waveform of current v/s deposition time for pulsed electrodeposition.

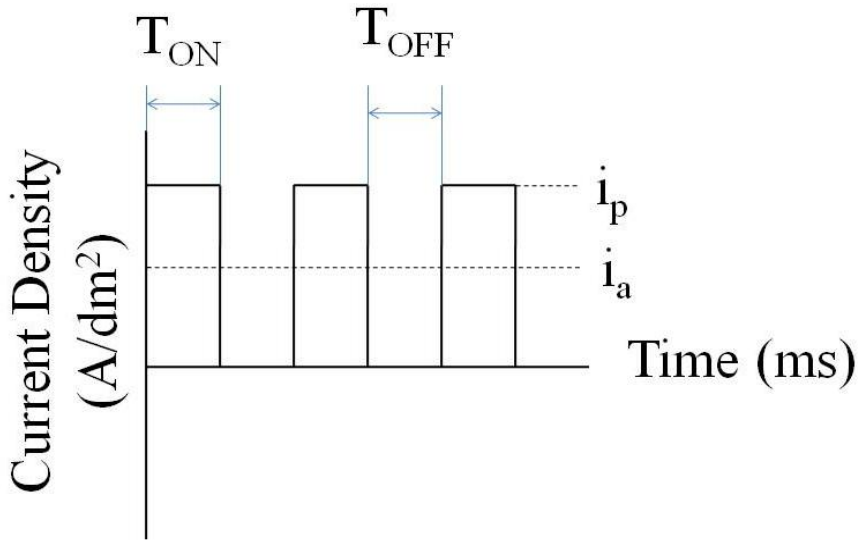

Fig. 2.4 *Schematic of pulse current waveform [35].*

Pulse electrodeposition helps in reducing porosity, lowering the level of inclusions and even higher deposition rates are possible compared with direct current deposition process. Pulsed electrodeposition is used for producing various nanocrystalline metals, alloys and composites successfully [9]. Pulse electrodeposition controls the microstructure and composition of deposited alloys or metals by effectively varying the pulse frequency (f), pulse length- current on time (t_{on}) -

the time between the pulses- current off-time (t_{off}), peak current density (I_p), average current density (I_a) and the duty cycle (θ). I_p represents the amount of current passing during on-time. The relation between these parameters is given as

$$I_a = \frac{I_p T_{on}}{T_{on} + T_{off}}; \qquad f = \frac{1}{T_{on} + T_{off}}; \qquad \theta = \frac{T_{on}}{T_{on} + T_{off}};$$

Pulsed current deposition has advantages over direct current in controlling the deposit grain size, shape morphology and preferred orientation which has significant effect on improving tribological and mechanical properties of the deposits [34].

2.3 Effect of Pulse Parameters on the Deposition Process

In pulsed electrodeposition, we have three independent parameters which can be varied namely the pulse on-time (T_{ON}) & off-time (T_{OFF}), pulse frequency (f) and the peak current density (I_P). These parameters not only influence the properties of deposit, but also have a considerable effect on the rate of deposition. Variation of any of these parameters has a considerable effect on the properties of the deposited coating.

2.3.1 Current Density

Current density is one of the important factors controlling the electrodeposition process. It has a strong influence on the deposition rate, plating quality and adherence of the plating. The higher the current density the faster the deposition rate, but the deposit obtained will be of poor quality and is less adherent at high current densities. Effect of current density on the deposition of wide range of materials has been investigated. Paatsch *et al*. [58] and Puippe *et al*. [59] observed that in metal plating increasing current density results in a decrease in the crystallite size of the deposit.

This is attributed to the high over potential associated with high peak current density. In alloy plating, a rise in current density tends to shift cathode potential to more negative value favoring the deposition of less noble metal; higher current density increases the rate of deposition of less noble metal forming thicker coatings. Ganesan *et al*. [67] studied the effect of current density on the deposition of Zn-Ni system and observed that Zinc content increases with increasing current density as shown in Fig. 2.5. Krishnappa *et al*. [60] investigated the effect of current density on alloy films and reported a rise in plating thickness with rising current density.

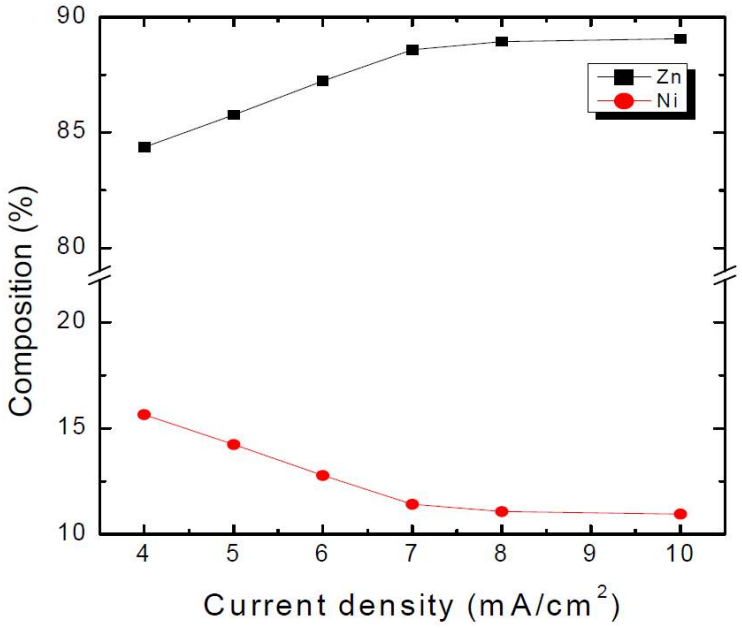

Fig. 2.5 *Effect of current density on zinc and nickel compositions of alkaline Zn-Ni deposits [67].*

2.3.2 Duty Cycle

Systematic investigations should be carried out in order to assess the effect of duty cycle on the deposition process. On increasing the pulse duty cycle, pulse on-time increases and off-time

decreases. This implies that at lower duty cycles, peak current flows for lesser time and hence the plating thickness is lesser than that obtained at higher duty cycles. Deposits which are less adherent and having considerable porosity will result at such parameters. Rehrig *et al*. [62] reported that grain size is also reduced at higher duty cycle. This is due to greater overpotential which is developed at longer pulse on-time leading to generation of more number of nucleation sites. Yoshimura *et al*. [68] measured the change in overpotential with increasing duty cycle during PED of palladium and found that it increases at longer pulse on-times. Few other researchers reported grain coarsening with increasing duty cycle and this is explained to be because of the decrease in overpotential with increased on-time. This illustrates that the effect of duty cycle on the properties of deposit also depends on the electrocrystallization process which is system dependant; it cannot be generalized for all the systems. Pulse duty cycle is generally coupled with pulse frequency for better results [64][67].

2.3.3 Pulse Frequency

Pulse frequency is also an important parameter responsible for the efficiency of the deposit obtained. It is defined as the reciprocal of the cycle time. At higher frequencies, short pulses pass through the material (as on-time is less) resulting in the formation of a thin pulsating diffusion layer. This thin layer favors higher nucleation rate and hence fine grained denser deposits with reduced porosity and higher hardness can be obtained. Shanti *et al.* [63] demonstrated the effect of pulse parameters on the electrodeposition of silver alloy. Fig. 2.6 gives the effect of pulse duty cycle on the current efficiency of silver plating. They reported a detailed study of the properties of silver deposit with variation of pulse parameters. Methodological approach should be used to optimize the pulse frequency and duty cycle to get best properties in any particular system.

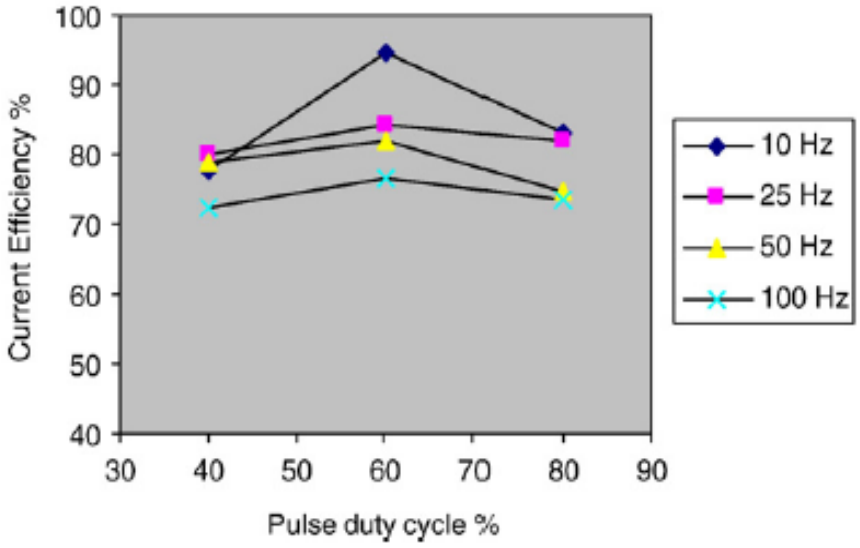

Fig. 2.6 *Effect of pulse duty cycle on the current efficiency [63].*

2.4 Cobalt and its Alloys – A Review

2.4.1 Cobalt Alloys

Cobalt alloys are recognized as a category of alloys which are wear resistant, corrosion resistant and heat resistant. The main factors contributing to these properties of cobalt are its crystallographic nature; solid solution strengthening effects produced by chromium, tungsten, and molybdenum; tendency to form metal carbides; and resistance to corrosion rendered by chromium [54][56]. Cobalt alloys find applications in components that require wear resistance, corrosion resistance, high temperature properties (especially strength at elevated temperatures), and magnetic properties. They are of particular interest to wear resistant applications because of the presence of hard phase precipitates, increasing the wear resistance of the component considerably. Although cobalt is alloyed with nickel and nickel-base alloys for high temperature applications, cobalt alloys also play an important role in high temperature resistance by virtue of their resistance to sulfidation and high temperature.

Cobalt can be alloyed with a large number of elements easily; it undergoes transformations forming solid solutions and intermediate phases. Among the several binary alloys possible, cobalt-aluminum, cobalt-copper, cobalt-tungsten and cobalt-silicon, are important for industrial applications because of their superior properties like high strength, ductility, stability at elevated temperatures, etc depending on the alloying element.

All these factors contribute to the use of cobalt and its alloys in demanding applications. The properties of Co-W alloys rendering them competitive among the hard chrome replacements will now be discussed.

2.3.2 Electrodeposited Cobalt-Tungsten Alloys

Cobalt-tungsten alloy deposits having better properties and higher tungsten content (upto 25%) can be obtained using a cobalt suphate – cobalt chloride – boric acid bath to which sodium tungstate is added. Tungsten content in the deposit can be increased by increasing the current density, deposition temperature and pH of the electrolyte. Cobalt-tungsten deposit forms as a solid solution which undergoes precipitation hardening on heat treatment. The properties of Co-W alloys produced by electrodeposition process will now be reviewed.

Microstructure

Structure of the Co-W alloy film (amorphous/crystalline) mainly depends on the tungsten content in the coating. Watanabe *et al.* clearly demonstrated the change in nature of the film coated with varying tungsten content. He has observed that the films containing less than 24.8 % W are crystalline and those containing more than 25.4 % W are amorphous [40]. Fig. 2.7 gives the X-Ray diffraction patterns of electroplated Co-W alloy films with various amounts of W. The

compositional range of various crystalline and amorphous phases observed in the X-Ray diffraction analysis can be understood using the equilibrium phase diagram (Fig. 2.8). Subsequent studies reported that amorphous Co-W coatings possess better properties when compared to the crystalline ones as discussed in the later part of this section.

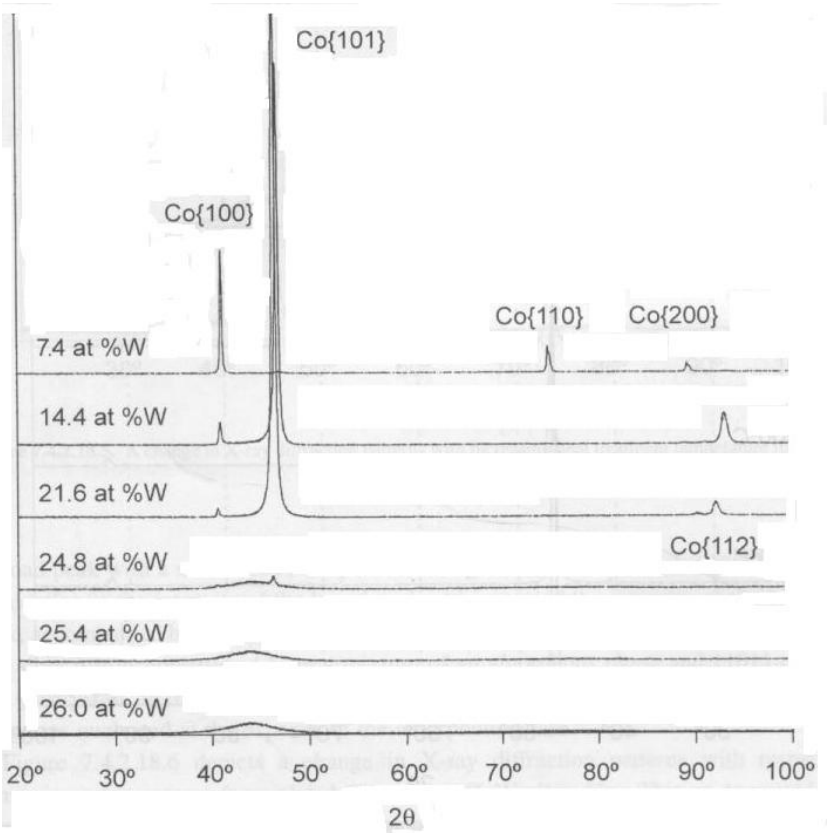

Fig. 2.7 *X-ray diffraction patterns of plated Co-W films with varying tungsten content [40].*

Phase Diagram

Fig. 2.8 shows the phase diagram of the Co-W alloy system. It shows different phases obtained as a result of solubility of W in Co over a wide range of temperatures and compositions, namely α-Co, ε-Co, Co_3W (intermediate phase), Co_7W_6 (intermediate phase) and W.

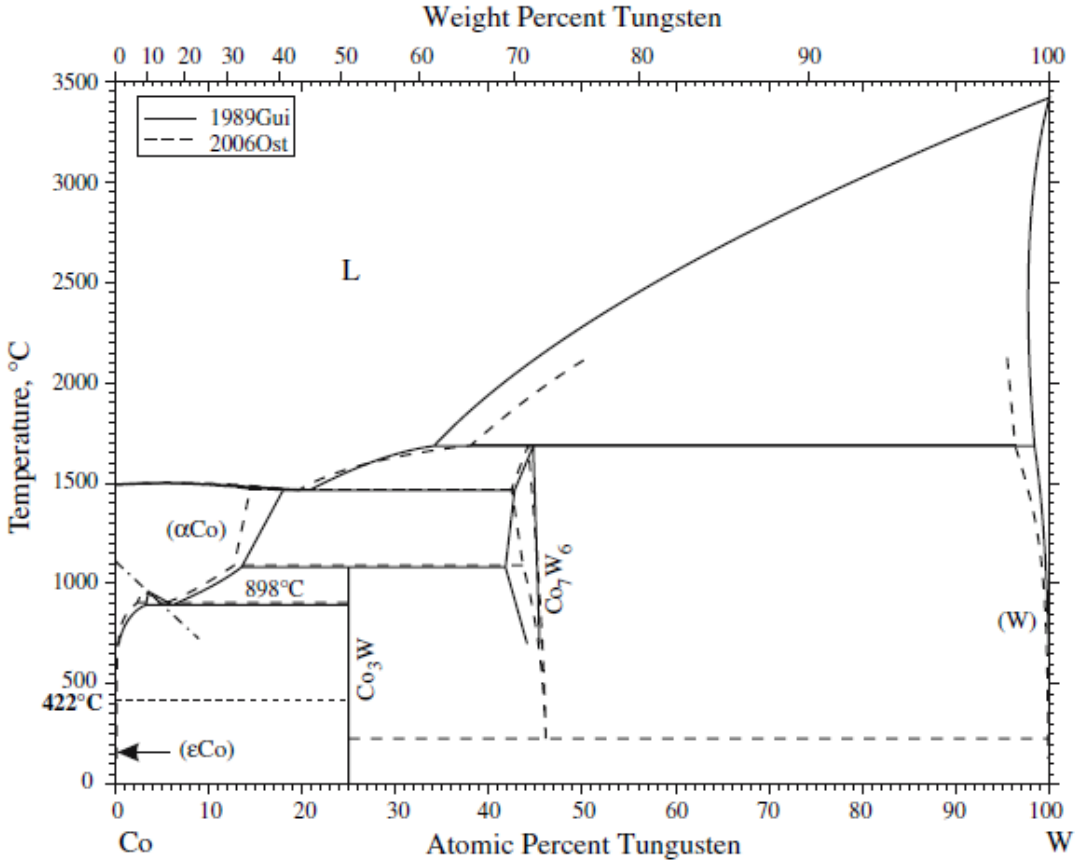

Fig 2.8 *Phase Diagram of Co-W alloy system [69].*

The phase diagram helps to identify the phases present in the resultant deposit, depending on the relative proportions of cobalt and tungsten and the parameters used. It also helps in understanding the nature of the deposit (crystalline or amorphous).

Hardness

Hardness of electrodeposited Co-W ranges from 500 to 700 kg/mm^2 depending on the cobalt and tungsten contents in the deposit giving different phases (seen in phase diagram in Fig. 2.8) and

also the operating conditions. Table 2.1 gives the microhardness of cobalt, tungsten and related compounds which can be possibly formed during electrodeposition or heat treatment process.

Table 2.1 Microhardness of Co and W and their compounds [74]

Material	**Microhardness (kg/mm^2)**
Co	130
W	350
Co-W	400-650
WC and W2C	1700-1800
CoO	380

Wear Behavior

Co-W alloy coatings show better wear resistance than chromium and pure cobalt coatings [70]-[85]. Weston *et al.* [81] investigated the tribological behavior of the nanostructured Co-W alloy coatings in comparision to pure Co and chromium ones. They found that amorphous Co-W alloy coatings exhibited low coefficient of friction and inturn better wear resistance as shown in Fig. 2.9 and 2.10. They clearly demonstrated that amorphous Co-W coatings exhibited better wear resistance in both dry sliding and lubricated conditions.

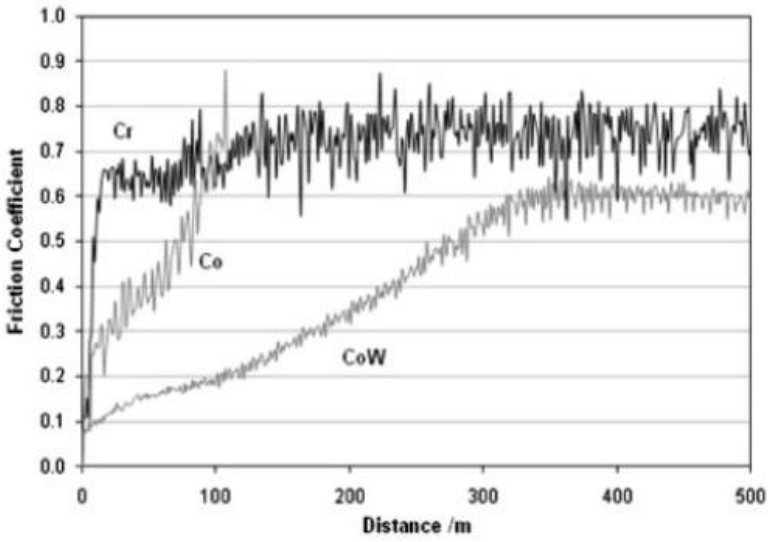

Fig. 2.9 *Coefficients of friction of three electrodeposits (Co-W, Co and Cr) sliding against 440C steel counterbody at a load of 61N [81].*

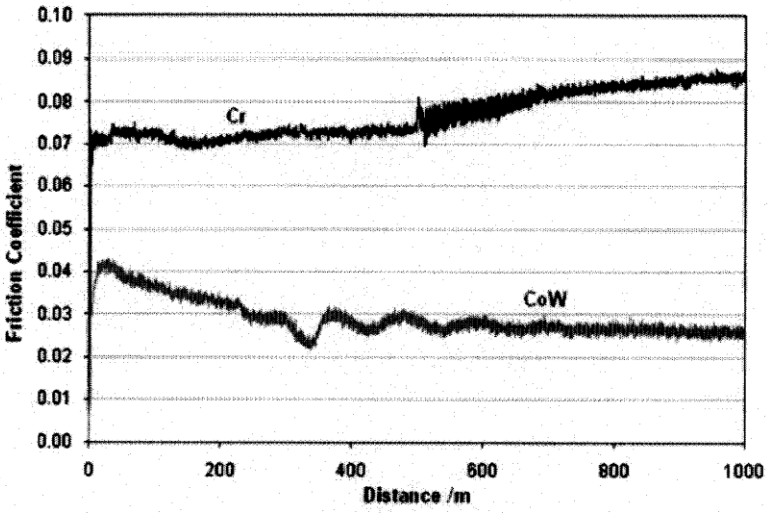

Fig. 2.10 *Variation of coefficients of friction with sliding wear in lubricated wear test on Co-W and Cr coatings at a load of 61N [81].*

The improvement in microhardness as well as wear resistance of these coatings mainly depends on intermediate phases formed during electrodeposition which promotes the grain refining and precipitation strengthening effect.

Corrosion Behavior

It has been proved by several investigators that Co-W coatings protect the underlying substrate from corrosion better than the hard chrome deposit. Hamid *et al.* [72] conducted salt spray corrosion tests of Co-W films and found that no corrosion product has formed until 72 hours proving them to be more efficient than the chromium coatings. Weston *et al.* [81] investigated the potentiodynamic behavior of the crystalline and amorphous Co-W coatings and found that crystalline ones exhibited better corrosion resistance than the amorphous ones. Fig. 2.11 shows the potentiodynamic plots for crystalline and amorphous coatings. This behavior is attributed to the point that segregated nanocrystalline matrix is more stable than the randomly distributed amorphous material making it more resistant to corrosion.

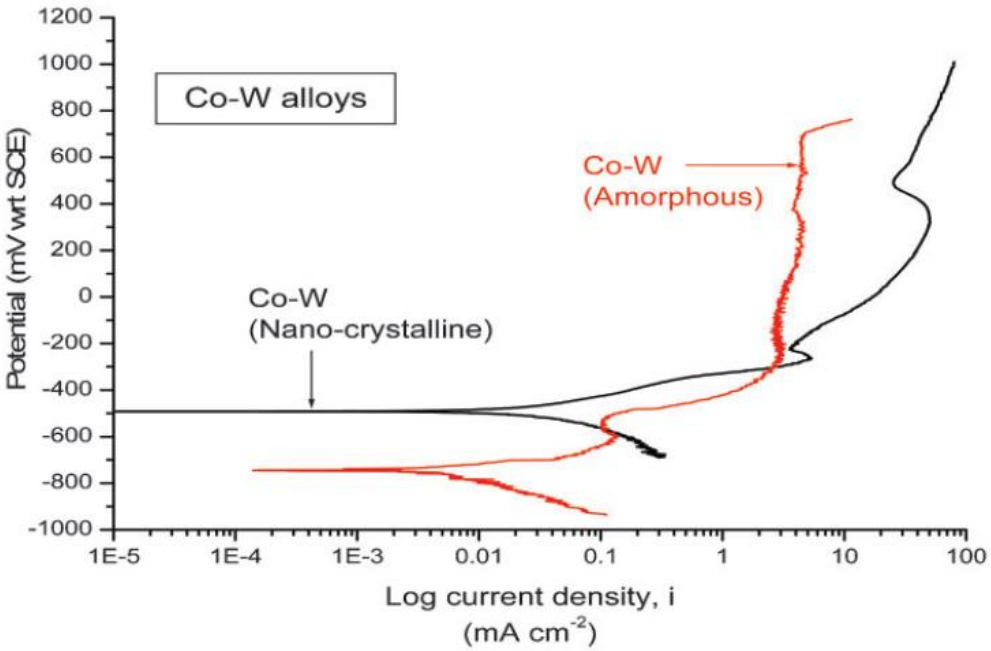

Fig. 2.11 *Potentiodynamic plots of amorphous and nanocrystalline Co-W coatings in 0.5M NaCl at 30°C [81].*

CHAPTER III

EXPERIMENTAL DETAILS

3.1 Citrate Bath

Electrolytic Co-W coatings were deposited using the citrate bath as electrolyte. It is prepared by dissolving analytical grades of cobalt sulphate heptahydrate ($CoSO_4.7H_2O$), sodium tungstate dihydrate ($Na_2WO_4.2H_2O$), boric acid (H_3BO_3), tri-sodium citrate ($Na_3C_6H_5O_7$), and citric acid ($C_6H_8O_7$) in distilled water. Table 3.1 shows the chemical composition of the electrolyte used for making 1 lt. of the electrolyte.

Table 3.1 Typical composition of citrate bath used for electrodeposition

Bath Composition	**Concentration (g/l)**
$CoSO_4.7H_2O$	56.2
$Na_2WO_4.2H_2O$	66
H_3BO_3	40
$Na_3C_6H_5O_7$	64.5
$C_6H_8O_7$	7.68

Citrate bath is chosen because of its inherent low toxicity, making the process more environmental friendly. It produces higher tungsten contents in the deposit, resulting in better mechanical properties of the plated alloy. Also, tri-sodium citrate used functions as a complexing agent, brightening and leveling agent, thus eliminating the need of other additives. Citric and boric acids act as primary and secondary buffers to maintain the pH of the electrolyte especially at the surface of the electrode within the recommended range (6.7±0.l in this case). The electrolytic bath was stirred continuously for 1 hour in order to obtain a homogeneous mixture. The pH of bath is maintained at 6.7 by adding sodium hydroxide to the solution.

3.2 Pulsed Electrodeposition (PED) Set-up

The electrodeposition was conducted by using Microstar pulse series power supply equipment mode 20-10-30 (Dynatronix, Amery, WI) shown in Fig 3.1. This pulse generator has the capacity to produce a maximum voltage of 20V and peak current of 30A. Minimum pulse width of 0.1 millisecond is possible in this series with a typical pulse rise and fall times limited to 50 microseconds. Also, maximum frequency of 10,000 Hz can be attained. While conducting experiment, one can vary the duty cycle, current density, frequency and duration of the test to desired values using this set-up and the adjusted values appear in the corresponding displays shown in Fig. 3.1.

Fig 3.1 *Pulse electroplating power supply.*

Electrolytic Cell and Surface Preparation

Stainless steel sheets, with surface area ~3.0 cm^2, were used as substrate materials (cathode) for deposition. The average Vickers microhardness of the substrate is in the range of 200 - 240 HV. A platinum plate was used as an anode. Before each experiment steel cathode was mechanically polished with different grade emery papers (400, 800 and 1200 mesh) successively. The substrates were then cleaned successively with acetone and distilled water with final rinsing in 10% H_2SO_4 to remove any residual alkali and to activate the surface just before electrodeposition. The electrodes were introduced into the electrolytic cell. The schematic showing electrolytic cell and the actual set-up of the electrodeposition process are shown in Fig. 3.2 and Fig. 3.3 respectively.

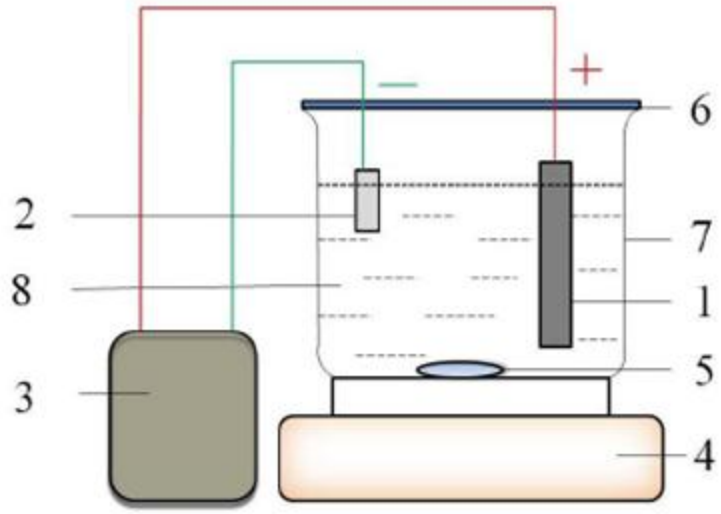

Fig. 3.2 *Schematic diagram showing different components of the electrolytic cell. 1. Platinum Plate, 2. Stainless Steel Plate, 3. Pulse Generator, 4. Hot Plate Stirrer, 5. Stirring Bar, 6. Locating Plate, 7. Beaker, and 8. Electrolytic Bath.*

Fig 3.3 *Laboratory experimental set-up used for fabrication of Co-W coatings.*

3.3 Processing of Co-W and its Composite Coatings

3.3.1 Investigations on the PED of Co-W Alloys

The Co-W coatings are coated on the stainless steel substrate using the citrate bath detailed above. The plating temperature is maintained at 58 °C and the pH is maintained at about 6.7 by adding sodium hydroxide. The plating time is maintained at 20 min. These are found to be the optimum electrodeposition parameters that yielded well adherent Co-W coatings on steel substrates. Further, pulse duty cycle (T_{ON} and T_{OFF}) and frequency are optimized to obtain amorphous Co-W coatings have better properties. This optimization is carried out through a series of experiments in which various combinations of pulse duty cycles (3.3% to 66.6%) and pulse frequencies (33 Hz to 333 Hz) are used at an average current density of 0.5 Adm^{-2}. Table 3.2 gives the list of parameters used for fabrication of coatings.

Table 3.2 Table showing variation of parameters of the electrodeposition

Duty Cycle (%)	**Frequency (Hz)**	**T_{ON} (ms)**	**T_{OFF} (ms)**
3.3	33	1	29
6.67	33	2	28
33.3	33	10	20
66.67	33	20	10
33.3	3.3	100	200
33.3	66.67	5	10
33.3	333	1	2

3.3.2 Synthesis of Co-W-Al_2O_3 Composite Coatings by PED

The plating electrolyte for the electrodeposition of the nano-alumina reinforced Co-W coatings consists of nano alumina particles (of particle size ~ 40nm) suspended in the citrate bath. Table 3.3 shows the chemical composition of the electrolyte used for making 1 lt. of the electrolyte.

Table 3.3 Typical composition of citrate bath used for electrodeposition

Bath Composition	**Concentration (g/l)**
$CoSO_4.7H_2O$	56.2
$Na_2WO_4.2H_2O$	66
H_3BO_3	40
$Na_3C_6H_5O_7$	64.5
$C_6H_8O_7$	7.68
Al_2O_3 (size ~ 40nm)	10

The electrolyte was kept stirring at a constant speed of 110rpm for 12hours before conducting the experiment to ensure homogeneous dispersion of alumina particles in the electrolytic bath. The electrodeposition set-up and the cell is similar to that used for deposition of Co-w coatings. Electrodes were introduced into the electrolytic cell in which the electrolyte is kept stirring constantly. The electrolyte is kept stirring constantly throughout the deposition process in order to prevent agglomeration of the alumina particles in the electrolytic bath. The plating temperature was maintained at 58^oC. The bath was maintained at pH 6.70 by adding sodium hydroxide and the volume of the bath is adjusted during the plating time by additions of distilled water. The electrodeposition process was carried out at an average current density of 1 to 9 A/dm^2, in intervals of 2A/dm^2 by maintaining the T_{ON} time equal to 1ms and T_{OFF} time equal to 2ms. Electrodeposition was carried out for 2hours at a frequency of 333Hz and at 33% duty cycle.

These were the optimum conditions to be maintained in order to obtain well reinforced homogeneous coatings. After electrodeposition for 2 hours, the coatings are cleaned in distilled water and dried before carrying out any kind of investigation on the same.

3.4 Characterization of Coatings

3.4.1 Microstructural characterization

The surface morphology of the coatings on the surface and cross-section are investigated using the scanning electron microscope (JSM-6370, JEOL). Microstructural analysis of the coatinsg is carried out using the SEM images obtained. The composite coatings are also etched in a etchant made using 25ml water, 25ml acetic acid and 50ml nitric acid. This is done to observe the grain boundaries more clearly under the SEM which gives us a clear idea about the grain size and grain structure of the composite coatings. It also helps us in ob serving the manner in which the alumina particles are reinforced into the Co-W alloy matrix giving us an idea of the probable mechanism of reinforcement.

3.4.2 Compositional and Phase Analysis

Elemental composition of the coatings were investigated using the scanning electron microscope (JSM-6370, JEOL) equipped with energy dispersive x-ray spectroscopy (EDS). FEI Quanta 600 field-emission gun Environmental Scanning Electron Microscope with an Evex EDS X-Ray microanalysis system and HKL EBSD system is used for EDS analysis.

In order to identify the structure and phases of the coatings, X-Ray diffraction analysis is carried out using Philips Norelco X-Ray diffractometer operating with Cu K_{α} (λ = 1.54178 Å) radiation at 20 kV and 10 mA. The diffraction angle was varied between 20° and 70° 2θ at a step increment of 0.02° and count time of 1 s during the analysis.

3.4.3 Surface Roughness

The surface roughness of pure Co-W coatings is measured using Mahr Perthometer model M1 (Model TR200, Micro Photonics^{TM}, Allentown, PA) which has a measuring range upto 150 μm. Detailed analysis of wear profile and depth of wear track of the composite coatings is carried out using PS50 Optical Profilometer (Nanovea, Irvine, CA) having optical pens with measuring range of 130 μm and 400 μm.

3.4.4 Characterization of mechanical properties

Micro and Nanomechanical Testing

A microhardness tester (Buehler^{TM}) was used to measure microhardness by performing indentations at a loading force of 10 gf and holding time of 10 s. At least 10 hardness measurements were conducted and average microhardness values for each sample are reported. Nanoindentation experiments were also carried out using Hysitron triboindenter which had a capacitive transducer with a load and displacement resolution of 1 nN and 0.002 nm, respectively. A standard diamond Berkovich indenter with a total included angle of 142.3^{o} and tip radius of around 150 nm was used. The nanohardness testing was carried out at a load of 2 mN and a loading rate of 40 μN/s. At least five indentations are taken on the film at this load and all the contact depths are found to be around 150 nm.

Nano-scratch experiments were also carried out using the same Berkovich indenter to find the value of coefficient of friction of the deposited coatings. The nano-scratch tests were conducted under constant force mode. The load function was set up in such a way that the indenter moves to 5 μm on either side of the rest position while applying a force of 1000 μN during the total scratch displacement of 10 μm. The total test duration was 54 s with each segment duration of 4s (the indenter moves a distance of 5 μm laterally during each segment). In the first 12 s indenter load was increased from 0 μN to 1000 μN which was then maintained. In

the next 30 s (until 42 s in total) constant load of 1000 μN was applied for the total displacement (both laterally and normally). The load was then reduced to 0 in 12 s completing the test.

Ball-on-disc Wear Testing

The micro-scale wear performance of the electrodeposited Co-W coatings was investigated by conducting sliding wear tests using ball-on-disk wear tester (Nanovea^{TM}, Irvine, CA). Here, a stationary ball with a defined normal force was pressed against the surface of the test sample mounted on a rotary disk. The samples were cleaned with distilled water, dried carefully, and then weighed before starting the wear tests. An alumina ball of 6 mm diameter was used as a counterbody.

The wear experiments were conducted under dry sliding conditions at room temperature with a load of 7 N and sliding velocity of 160 rpm. Each wear test was carried out for a total duration of 18 min. The weight loss of the coating was measured after every 3 min of wear test. The position of specimen on the tribometer was maintained after each weight loss reading such that wear continues on the same worn track during continued wear testing.

Characterization of Electrochemical Behavior

The corrosion resistance of the Co-W coating was studied by using a potentiostat/galvanostat VersaSTAT 4 (Ametek, Princeton Applied Research) which had maximum current capacity up to 1 A. In this study, we used tafel technique to determine the corrosion potential (E_{corr}), corrosion current (I_{corr}), and corrosion rate. For this, a three-electrode electrochemical cell was used. The Co-W coated sample was used as the working electrode; platinum was used as counter electrode; and the reference electrode was a saturated calomel electrode (SCE). The area of the working electrode was 1 cm^2. The reference electrode used was Ag/AgCl/saturated KCl (0.197 volts).

The corrosion properties of the coating were studied by polarization in 3.5% NaCl solution with pH ~7.0 at room temperature. The Co-W coatings were subjected to initial and final potential of -0.9 V and 0.5 V respectively. A constant potential scan rate of 0.167 V/s was employed during the test. The tafel polarization curves were plotted during the whole test with the given scan rate.

CHAPTER IV

FINDINGS

4.1 Effect of Pulse Duty Cycle and Frequency on Co-W Coating Characteristics

4.1.1 Surface Morphology

The SEM micrographs showing the effect of pulse duty cycle (for constant pulse frequency of 33 Hz) on surface morphology of coatings presented in Fig. 4.1 (a-d). The surface of the coatings deposited at lower duty cycles (3.3 and 6.67 %) shows well defined faceted pyramidal grains with uniform grain size (1-3 μm). The fraction of faceted grains decreases with increasing pulse duty cycle. The coatings deposited at intermediate pulse duty cycle (33 %) shows mixed surface microstructure with distributed faceted grains. At higher pulse duty cycle (66.67 %), the surface of coatings consists of coarse (~2 μm) colonies of fine granular features without any well defined facets. The effect of pulse frequency (for constant pulse duty cycle of 33%) on the surface microstructure is also shown in Fig. 4.1 (e-g). At lower pulse frequencies (3.3 and 66.67 Hz), the surface structure consisted of distributed colonies of fine granular features. The coating deposited with highest pulse frequency (333 Hz) exhibited well refined granular features with feature size in the range of 150-200 nm.

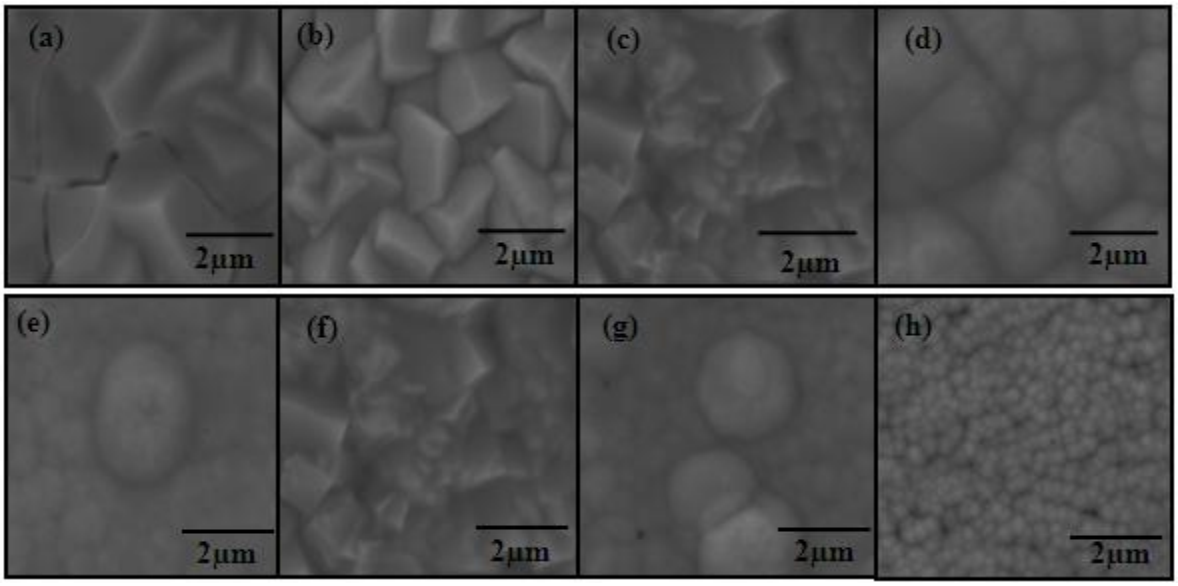

Fig. 4.1 *SEM micrographs of Co-W coatings electrodeposited with various pulse parameters: (a) f=33 Hz, θ=3.3 %, (b) f=33 Hz, θ=6.67 %, (c) f=33 Hz, θ=33.3 %, (d) f=33 Hz, θ=66.67 %, (e) θ=33.3 %, f=3.3 Hz, (f) θ=33.3 %, f=33 Hz, (g) θ=33.3 %, f=66.67 Hz, and (h) θ=33.3 %, f=333 Hz.*

It has been observed that thickness of all the coatings remained constant. It is found to be in the range of 10 – 12 μm throughout the cross-section of the coating as seen in Fig. 4.2 (a).

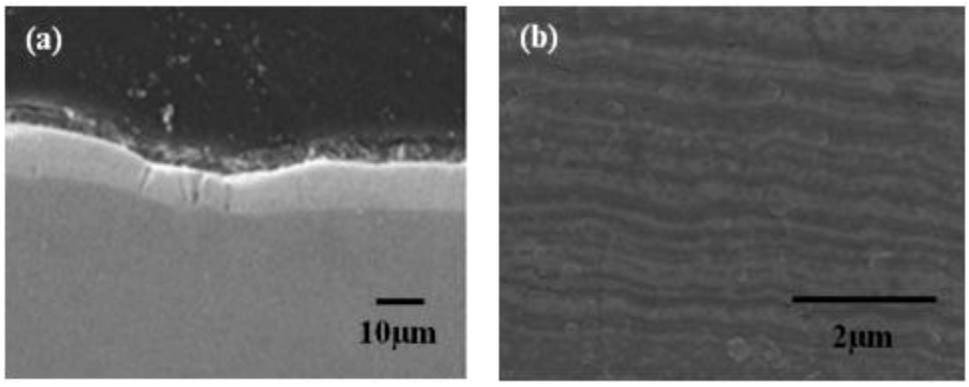

Fig. 4.2 *Cross-Sectional image at the interface between coating and substrate, detail of the nanostructure of coating obtained f=333 Hz), θ=33.3%.*

It can be inferred from the thickness data that the variation of pulse parameters has no significant effect on the thickness of the coatings. The coating time and current density are kept constant for all the parameters. The deposited Co-W coatings obtained from the citrate baths onto the steel substrate are adherent, compact and visually bright as observed from the cross sectional image in Fig 4.2 (a). Fig. 4.2 (b) shows the high magnification image of the cross-section of the coating. It clearly shows a compact coating with a layered structure.

4.1.2 Compositional and Phase Analysis

The elemental composition of the coatings deposited with various combinations of pulse duty cycles and pulse frequencies was determined using EDS. The variation of atomic percentages of major elements, cobalt and tungsten, with pulse parameters is shown in Fig. 4.3. For constant pulse frequency (33 Hz), the percentage of tungsten increased (from ~12 to 20 at. %) with increasing duty cycle (from 3.3 to 66.67 %). The effect of pulse frequency (with constant duty cycle of 33.3%) on the composition was not significant. The percentage of tungsten in the coatings remained close to ~18-20 at. % with increasing pulse frequency.

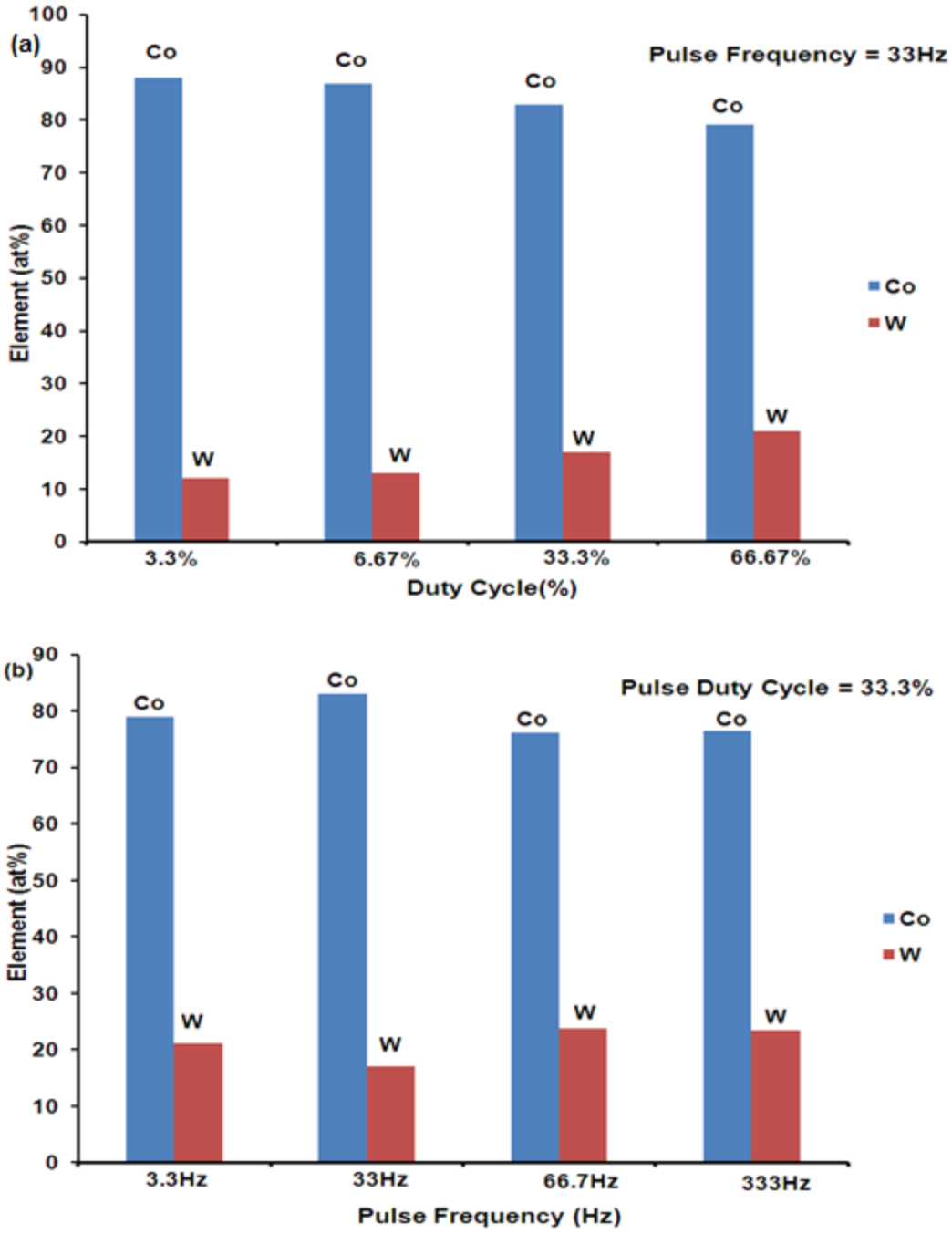

Fig. 4.3 *Variation in atomic percentages of cobalt and tungsten in Co-W coatings electrodeposited with (a) f=33 Hz and various pulse duty cucles, and (b) θ=33.3 % and various pulse frequencies.*

A typical elemental map of a Co-W coating surface is presented in Fig. 4.4. The figure shows the uniform distribution of constituent elements, Co and W, in the alloy coatings.

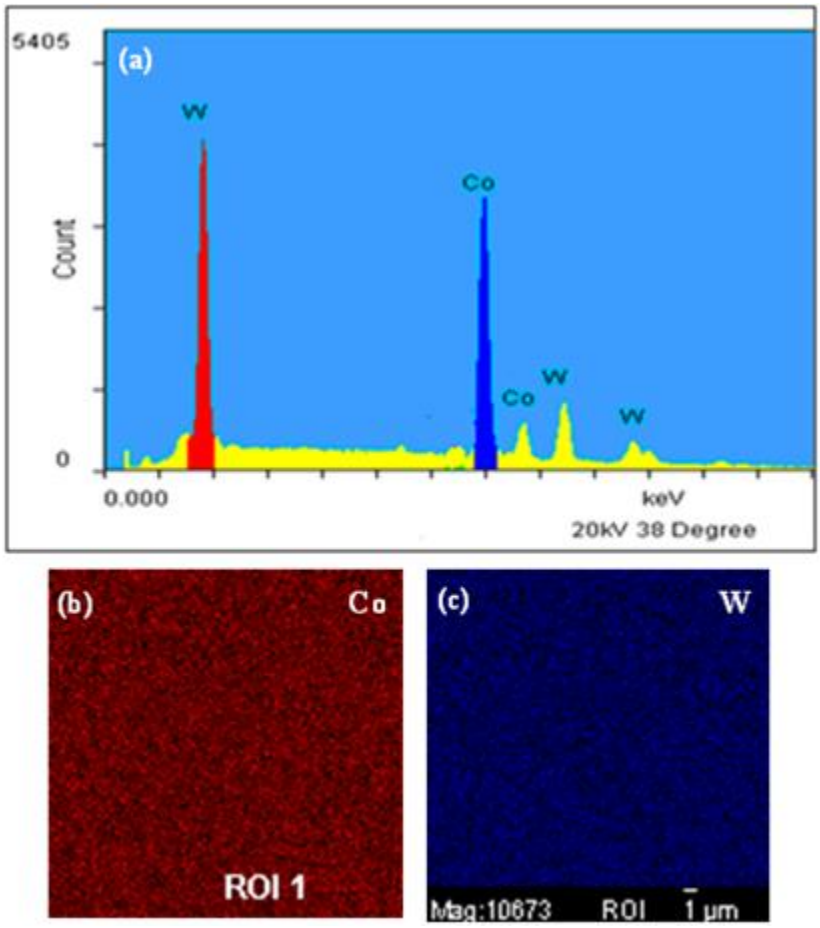

Fig. 4.4 *Elemental mapping of the surface of Co-W coatings electrodeposited with pulse current conditions (f=333 Hz and θ=33%).*

X-ray diffraction (XRD) patterns from the coatings deposited with various pulse duty cycles (for pulse frequency of 33 Hz) are presented in Fig. 4.5 (a). At lower duty cycles (3.3 and 6.67 %), the XRD patterns show sharp peaks indicative of crystalline structure of the coatings. This supports the observations of well-defined faceted surface grains for these coatings (Fig. 4.1 (a-b)).

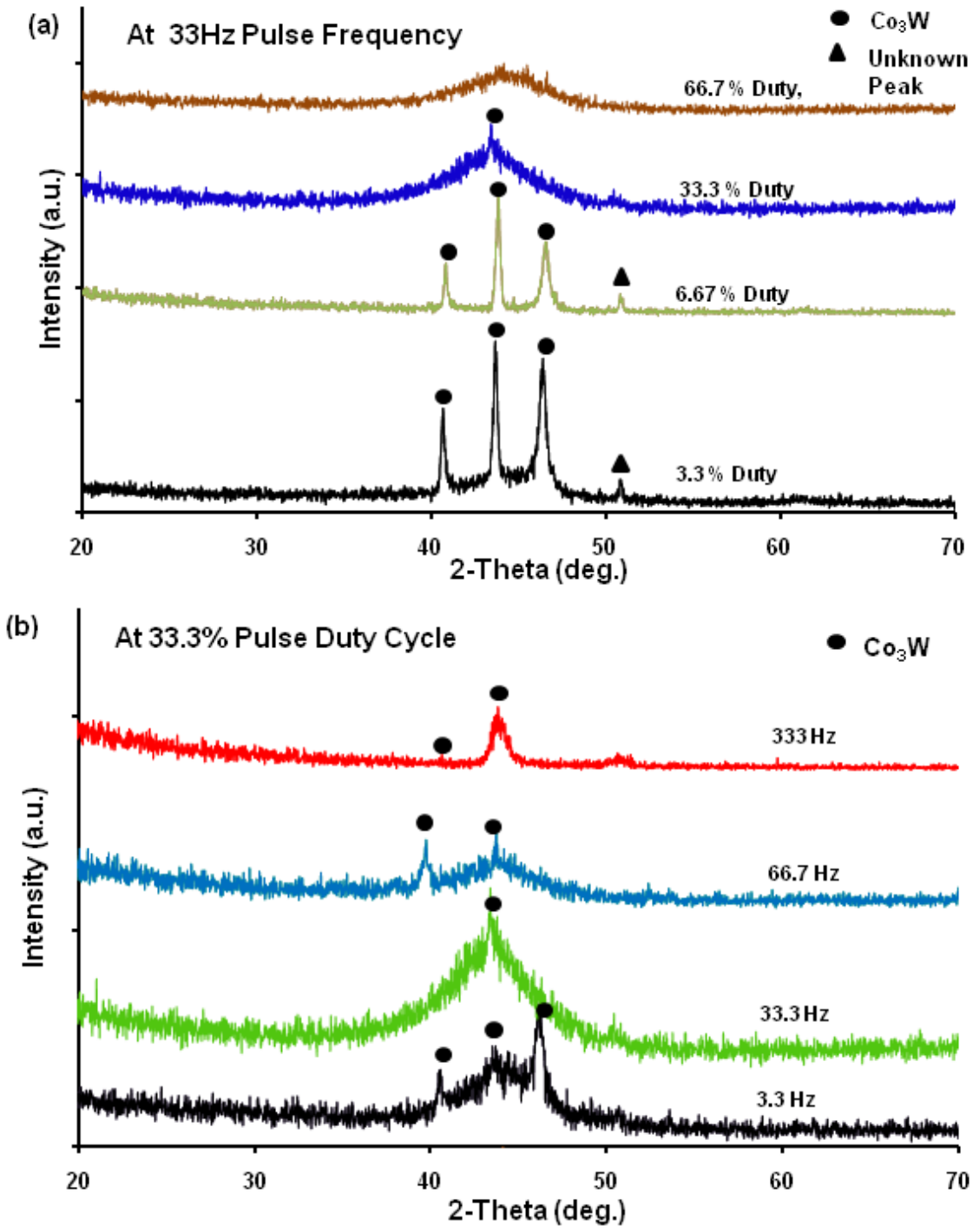

Fig. 4.5 *X-ray diffraction pattern of Co-W coatings electrodeposited with (a) f=33 Hz and various pulse duty cucles, and (b) θ=33.3 % and various pulse frequencies.*

At highest duty cycle (66.7 %), the XRD pattern exhibited broad peak, centered at 2θ~45°, indicative of the amorphous structure of the coatings. These coatings showed fine granular surface features (Fig. 4.1 (d)). At intermediate duty cycle (33.3 %), the XRD pattern exhibited a broad halo peak with a superimposed sharp peak. This indicates the presence of mixed amorphous and crystalline structure of these coatings. These coatings showed distributed faceted grains in the fine granular matrix (Fig. 4.1 (c)). The XRD patterns clearly indicate the transition from crystalline to amorphous coatings with increasing pulse duty cycle at constant pulse frequency. No such structural transitions were observed with increasing pulse frequency for constant pulse duty cycle of 33.3 % (Fig. 4.5 (b)). Most of these coatings showed broad peak with superimposed sharp peak indicative of mixed amorphous/crystalline structure of these coatings. At the highest pulse frequency (333 Hz with 33.3 % duty cycle), the XRD peak shows broadened sharp peak. This broadening of the peak seems to be due to nanostructured granular features in these coatings (Fig. 4.1 (d)). The three sharp peaks in the 2θ range of 40-50° matches with that for Co_3W hexagonal intermetallic phase (JCPDS: 02-1298). This is one of the major phases in the Co-W alloy system with tungsten content less than ~25 at.% (below 350 °C).

The formation crystalline or amorphous phases during electroplating of binary alloys is primarily determined by the electrode overpotential and composition. The electrode overpotential depends on pulse on-time and increases with increasing T_{on} time. In general, the rate of nucleation increases with increasing overpotential, resulting in finer crystals. Eventually at very high overpotential amorphous structure can be formed. It can be seen that the tendency to form amorphous structure for Co-W coatings increases with increasing pulse duty cycle (at constant pulse frequency of 33 Hz). This seems to be due to increasing electrode overpotential with increasing T_{on} time (the T_{on} time increases with duty cycle). The tendency to form amorphous structure also increases with increasing W content in the coating towards composition corresponding to intermetallic Co_3W (Co-25 at.% W). The Co-W coatings with less than ~15

at.% W are predominantly crystalline, whereas the coatings with greater than ~20 at.% W are predominantly amorphous. While similar observations on compositional dependence of crystalline-amorphous transitions in electroplated films have been made for Ni-S system [19], clear understanding of the atomistic mechanisms of film formation is not yet reached. Even though the composition of the coatings deposited with 33.3 % pulse duty cycle (at various pulse frequencies) were close to intermetallic Co_3W composition, these coatings did not exhibit fully amorphous structure. This is probably due to insufficient electrode overpotential with the complexity of pulse parameters.

4.1.3 Surface Roughness and Microhardness

The variation of surface roughness and microhardness of the coatings with pulse duty cycles at constant pulse frequency is shown in Fig. 4.6.

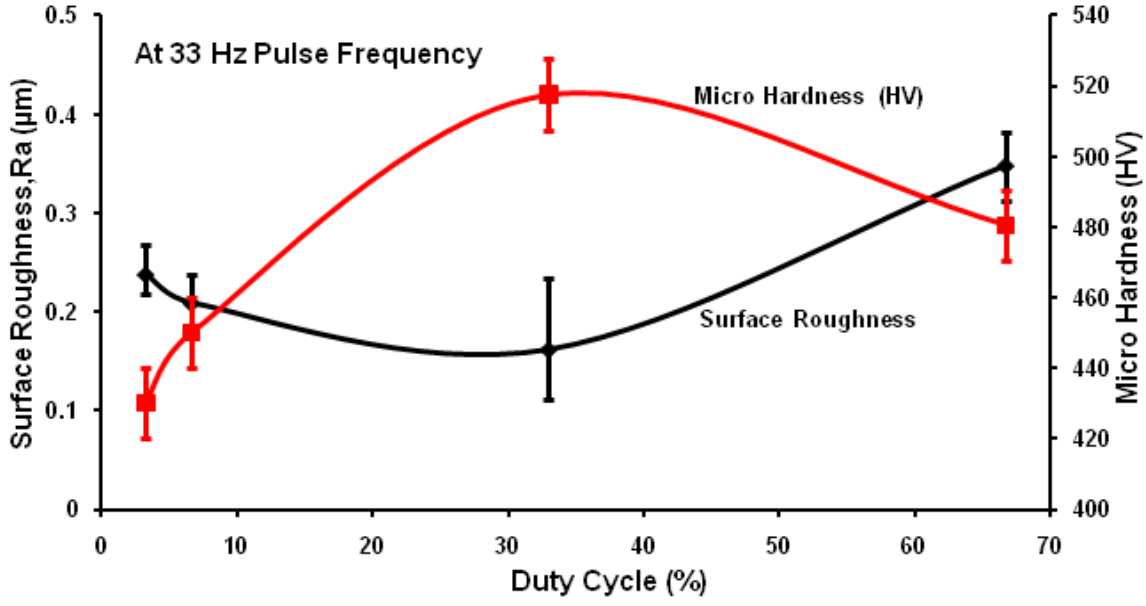

Fig. 4.6 *Effect of pulse duty cycle on surface roughness and microhardness of Co-W coatings deposited with constant pulse frequency (f=33 Hz).*

Even though all the coatings were smooth (surface roughness, Ra<0.3 μm), it can be observed that the surface roughness decreases, reaches minimum, and then increases with increasing pulse duty cycle. The higher surface roughness at lower (3.3 and 6.67%) and higher (66.67%) pulse duty cycles is primarily due to pyramidal faceted grains and coarse colonies of granular features of the coatings. The intermediate duty cycle (33.3 %) provides coatings with lowest surface roughness associated with distributed faceted grains in fine matrix. These coatings deposited with 33.3 % pulse duty cycle and 33 Hz pulse duty cycle also exhibit highest surface hardness (~510-530 HV). Note that these processing conditions resulted in amorphous/crystalline mixed structure with distributed faceted grain in the fine matrix. It seems that such microstructure gives better combination of high hardness and smooth surface. The Co-W alloys are often considered as potential candidates for replacing hard chromium coatings due to their environmentally benign processing. However, the hardness of the Co-W coatings (~510-530 HV) obtained with pulse processing conditions explained above is lower that that for hard chromium coatings (~700-850 HV). To realize the potential of these Co-W coatings, further improvements in the hardness are needed. We also investigated the effect of pulse frequency on the coating hardness and surface roughness keeping the duty cycle constant at 33.3 % (Fig. 4.7).

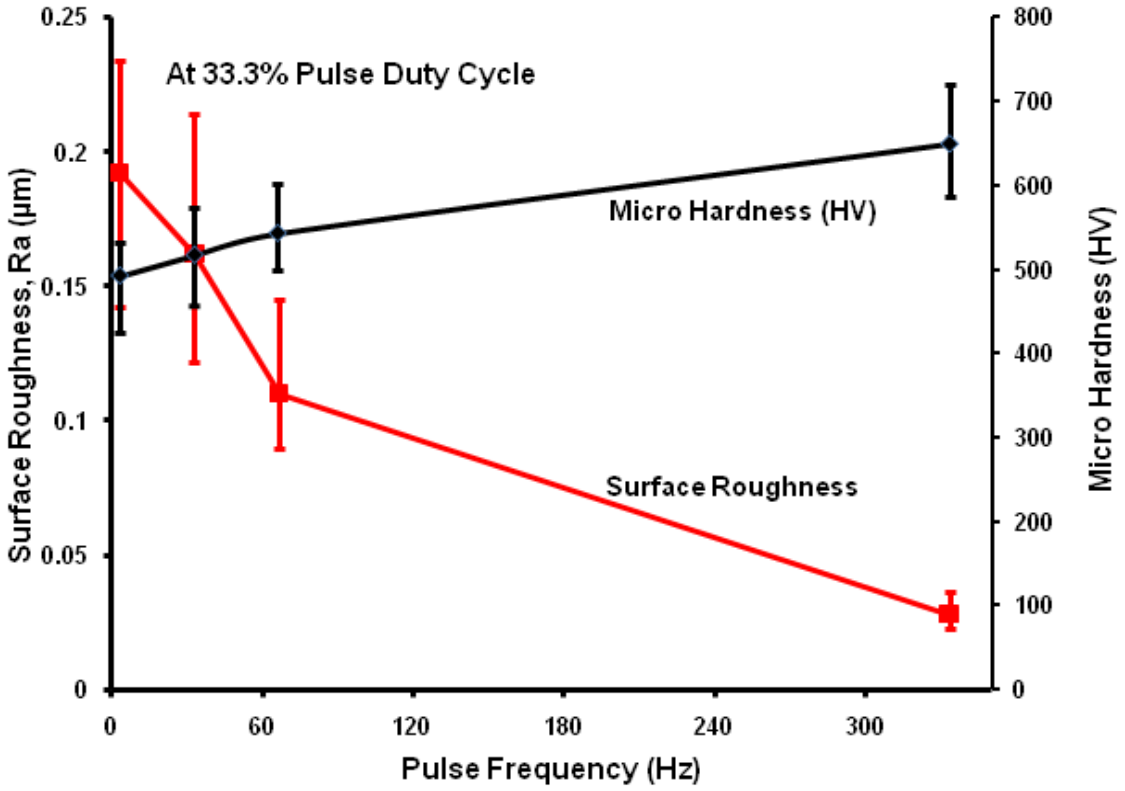

Fig. 4.7 *Effect of pulse frequency on surface roughness and microhardness of Co-W coatings deposited with constant pulse duty cycle (θ=33.3 %).*

Significant improvements in the hardness were observed with increasing pulse frequency (3.3-333 Hz). Furthermore, the surface roughness decreased with increasing pulse frequency. Due to complexity of observations, including variation of phases (relative fractions of amorphous and crystalline phases), composition (~12-25 at.% W and fraction of Co_3W intermetallic), microstructure (relative percentages of coarse colonies and refined matrix), and surface roughness (Ra~0.25 µm-25 nm) with pulse frequency, it is difficult to attribute the increasing hardness to any specific observation. The coatings prepared using 33.3 % duty cycle and 333 Hz pulse frequency exhibited best combination of high hardness (~575-725 HV) and smooth surface finish (Ra~25 nm). These coatings exhibited most refined nanostructured granular features (150-200

nm). While the surface hardness of these Co-W coatings is still at the lower end of the desired hardness range (~700-850 HV), the environmental advantages associated with their processing are expected to provide impetus towards using these coatings for hard chromium replacement.

4.1.4 Wear, Nano-mechanical and Electrochemical Properties of Co-W Coatings Deposited with 33.3 % Pulse Duty Cycle and 333 Hz Pulse Frequency

Micro-wear and Nano-scratch Testing

The sliding wear resistance of the as-deposited Co-W coatings and steel substrate was characterized using ball-on-disc wear testing with 160 rpm and 7 N normal force. Fig. 4.8 shows cumulative weight loss in both the Co-W coating and steel substrate as a function of sliding time. The total weight loss in the coatings over the entire duration of sliding wear test was almost half of that for steel substrate, indicating that the coatings have far better wear resistance compared to the substrate. This seems to be the direct result of higher hardness of the coatings. For the coatings, it can be noted that the wear rate (slope of the curve) increases after about 9 minutes.

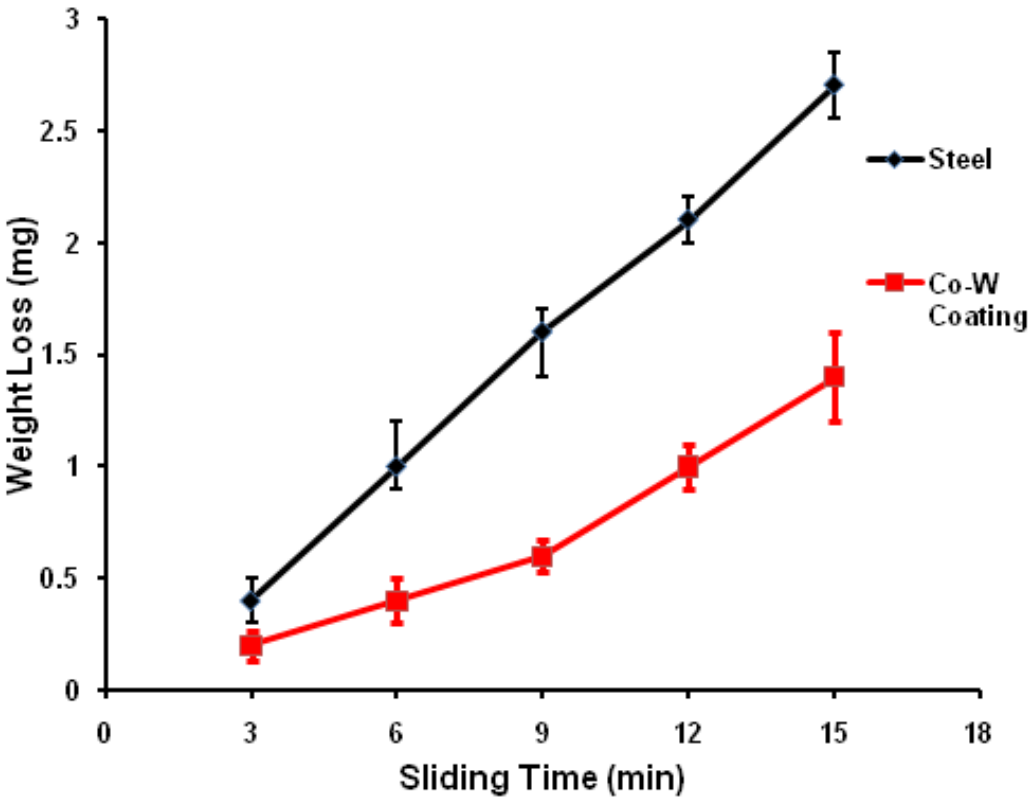

Fig. 4.8 *Cumulative weight loss of the Co-W coating (electrodeposited with f=333 Hz and θ=33 %) and steel substrate during ball-on-disc wear test.*

Fig. 4.9 shows the SEM micrographs from the worn surface after early and later stages of wear test. Both the SEM images show parallel micro-scratches along sliding direction characteristic of abrasive wear. The increase is wear rate in the later stage of wear test seems to be due to fragmentation of coating. Fig. 4.8 (b) clearly shows the regions of coating fragmentation and the accumulation of fine wear debris in the center of the wear track.

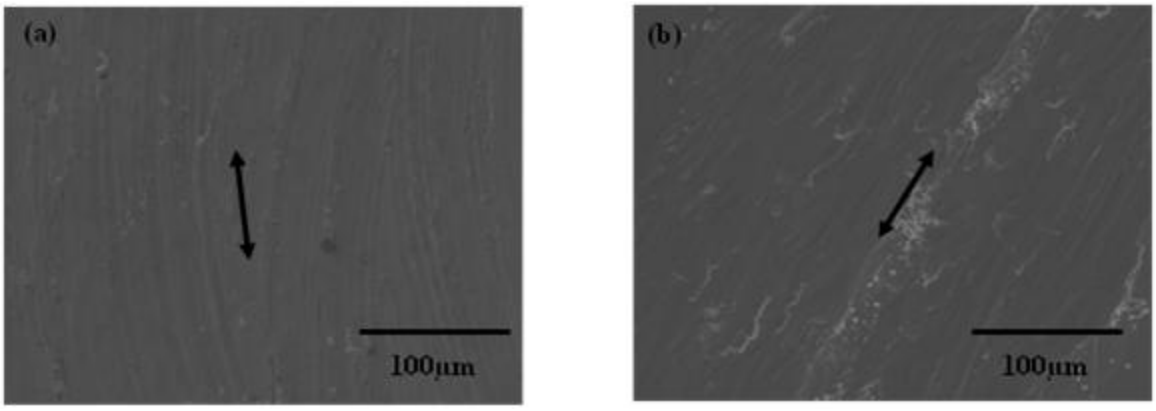

Fig. 4.9 *SEM micrographs from the worn surfaces of Co-W coatings electrodeposited with f=333 Hz and θ=33 % after (a) initial, and (b) later stages of wear testing (arrows indicate the sliding direction).*

Fig. 4.10 shows the variation of coefficient of friction with sliding time in early stages of wear. It can be seen that the coefficient of friction increases fairly linearly to about 0.45 within first 30 seconds and then stabilizes in the range of 0.4-0.5.

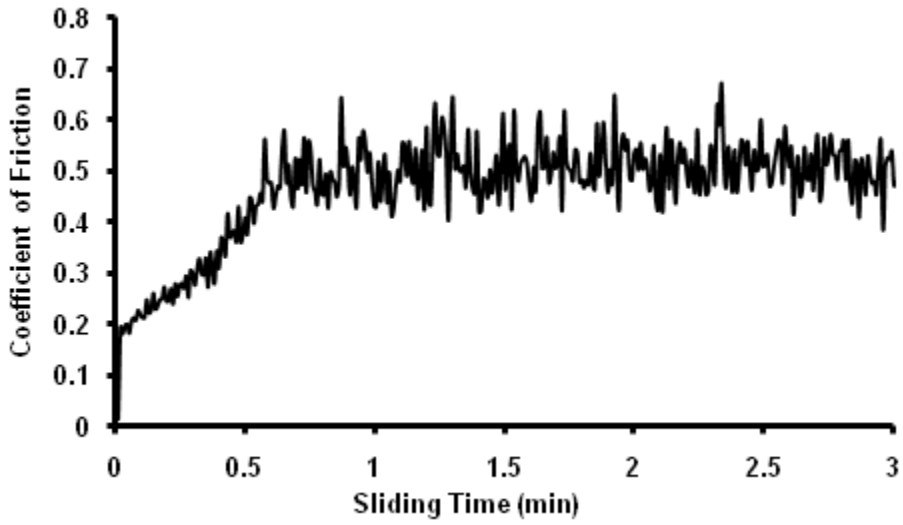

Fig. 4.10 *Variation of coefficient of friction with sliding time during ball-on-disc wear test of the Co-W coatings electrodeposited with f=333 Hz and θ=33 %.*

The mechanical properties of materials are significantly influenced by the length-scale over which the properties are measured. As discussed in previous sections, the coatings deposited with 33.3 % duty cycle and 333 Hz pulse frequency exhibited well refined granular features with feature size in the range of 150-200 nm. To investigate the influence of length scale on mechanical properties, nano-indentation and nano-scratch testing on these coatings was conducted. Nanohardness of the coating was obtained by applying a normal load of 2 mN, and loading and unloading rate of 40 μN/sec. Fig. 4.11 shows a typical load displacement curve associated with nano-indentation tests. The maximum depth associated with this nano-indentation test was 134.4 nm. With this testing, the coating nanohardness was found to be in the range of 5-10 GPa. While these nanohardness values are slightly lower than that for electrolytic chromium (maximum hardness: ~13 GPa), the hardness values are in good agreement with the existing literature of Co-W coatings [14].

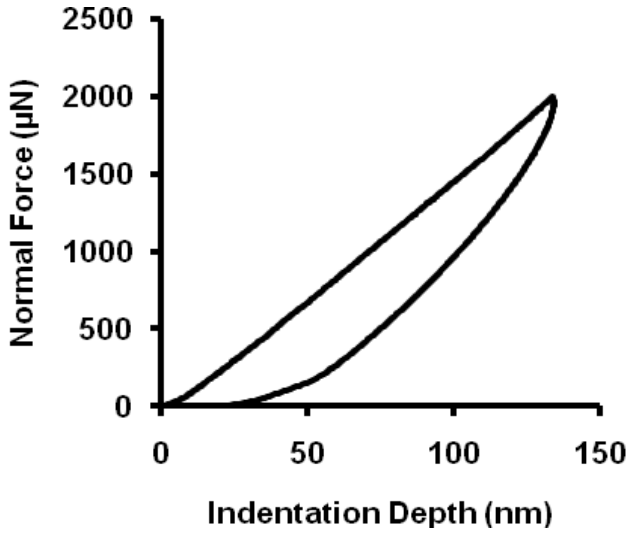

Fig. 4.11 *Typical load-displacement curve for nanoindentation of Co-W coating electrodeposited with f=333 Hz and θ=33 %.*

The nano-scratch tests were also performed on the Co-W coating to determine the coefficient of friction of the coating as shown in Fig. 4.12.

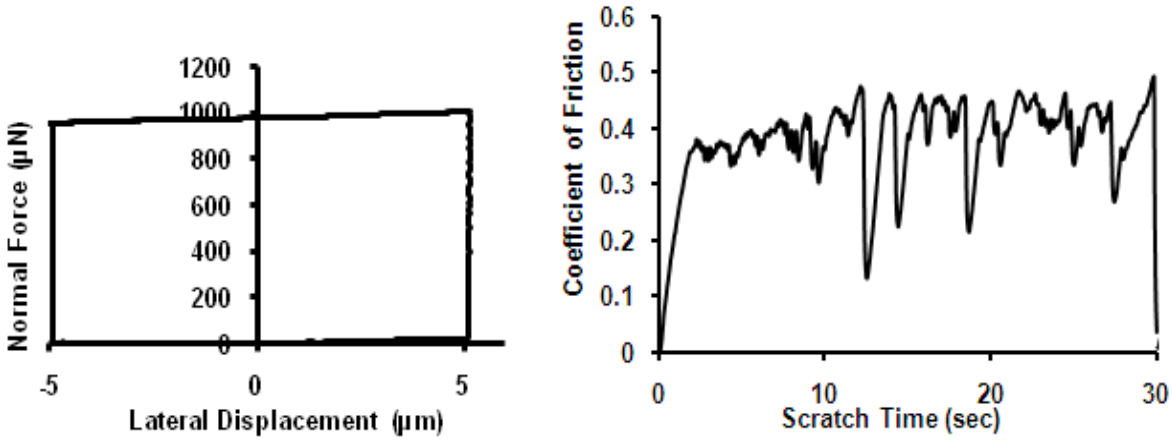

Fig. 4.12 *(a) Variation of normal force with total lateral displacement during nano-scratch, (b) variation of coefficient of friction with scratching time of 30 s for Co-W coating electrodeposited with f=333 Hz and θ=33 %.*

Fig. 4.12 (a) shows the variation of normal force with lateral displacement during nano-scratch testing. As shown in the figure, a constant force of 1000 µN was applied during scratching over a displacement of 10 µm (starting 12^{th} and ending 42^{ndth} second). Fig. 4.12 (b) shows the variation of coefficient of friction during scratch test. It can be seen that the coefficient of friction increases to about ~0.4 within first 2.5 s. Beyond this time, the coefficient of friction oscillates about 0.4. The initial oscillations seem to be due to nano-scale surface features (roughness) periodically obstructing the movement of nanoindenter. The amplitude of the oscillations was higher in the later stages of scratching. Note that the surface was scratched along same line (10 µm) multiple times during 30 s of scratch time. This higher amplitude of oscillations of coefficient of friction in later stages of scratching is probably due to re-scratching of the fragmented regions of the surface. The coefficient of friction obtained with nano-scratch

testing is slightly lower than that obtained with micro-wear tests. For these Co-W coatings, the length scale of measurement does not seem to significantly affect the coefficient of friction values.

Electrochemical Behavior

Fig. 4.13 shows the potentiodynamic polarization curve for Co-W coating obtained over the potential range of -0.9 V to 0.5 V.

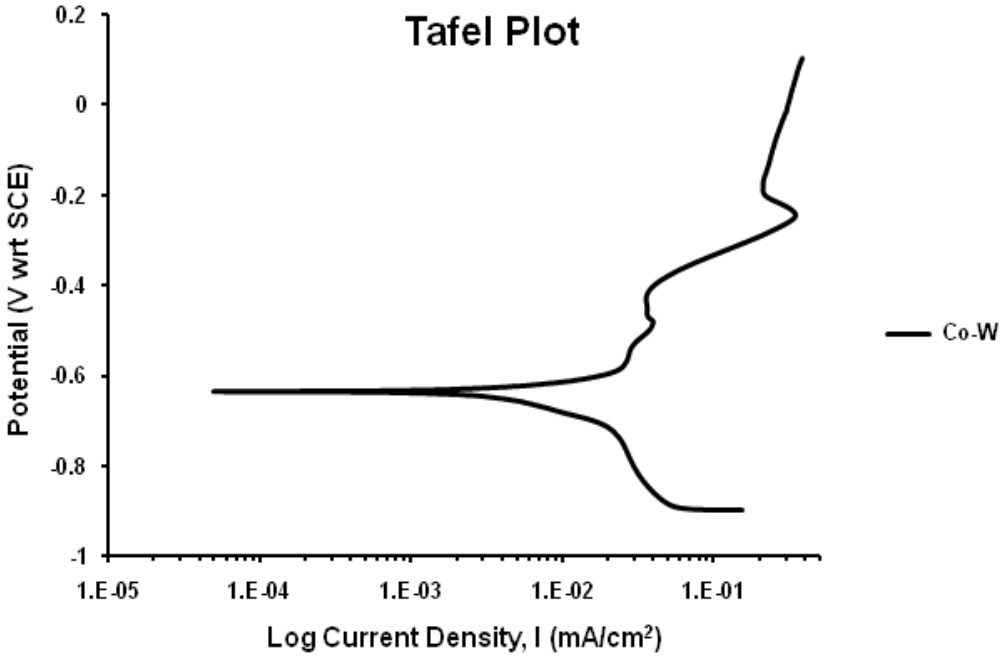

Fig. 4.13 *Tafel polarization curve for the Co-W coating (electrodeposited with f=333 Hz and θ=33 %).*

The corrosion potential (E_{corr}) and corrosion current (I_{corr}) for the as deposited Co-W coating was found to be -636.5 mV (SCE) and 88.7 μA, respectively. After the initial region of activation, the Co-W coatings undergo passivation between -620 mV and -430 mV. The wide

passive range for the Co-W coatings is indicative of the ability of the surface to withstand localized corrosion, such as pitting corrosion [81]. Tafel fit was also used to determine the corrosion current and the corresponding corrosion rate of the samples. The corrosion rate for Co-W coatings is very low in the range of 1.631 mpy indicating the corrosion resistance of the coating. Thus, the Co-W coatings exhibited significantly improved corrosion resistance. Tungsten being a more corrosion resistant component, improved corrosion resistance of the Co-W coatings can be attributed to the tungsten content of the coating.

4.2 Effect of Current Density on the Reinforcement of Alumina in Co-W Alloy Matrix and the Properties of Composite CoatingS

4.2.1 Structural Characterization and Grain Size Analysis

The surface morphology of pure Co-W coating deposited at 33% pulse duty cycle, 333Hz frequency and 1A/dm^2 current density is presented in Fig. 4.14 (a) and shows well refined granular features with the feature size in the range of 300-450 nm. The coating is found to be well adherent to the substrate having a thickness in the range of 8-10 μm as shown in Fig 4.15 (a).

The sample surface morphology of the composite coatings (reinforced with alumina) after etching as investigated using SEM is presented in Fig. 4.14 (b-f). A comparison of the microstructures of composite coatings at different current densities is shown. The surfaces of the coatings are compact without any pores or voids and this holds good for all the samples. Nano-alumina particles reinforced in the Co-W alloy matrix are observed near the grain boundaries of the Co-W alloy matrix (in the SEM images). The existence of alumina has also been confirmed from EDAX analysis which is discussed in the next section. The reinforcement of these nano alumina particles by electrodeposition can be attributed to the adsorption of alumina particles on

the cathode surface, followed by the deposition of the Co-W matrix around the adsorbed alumina particles.

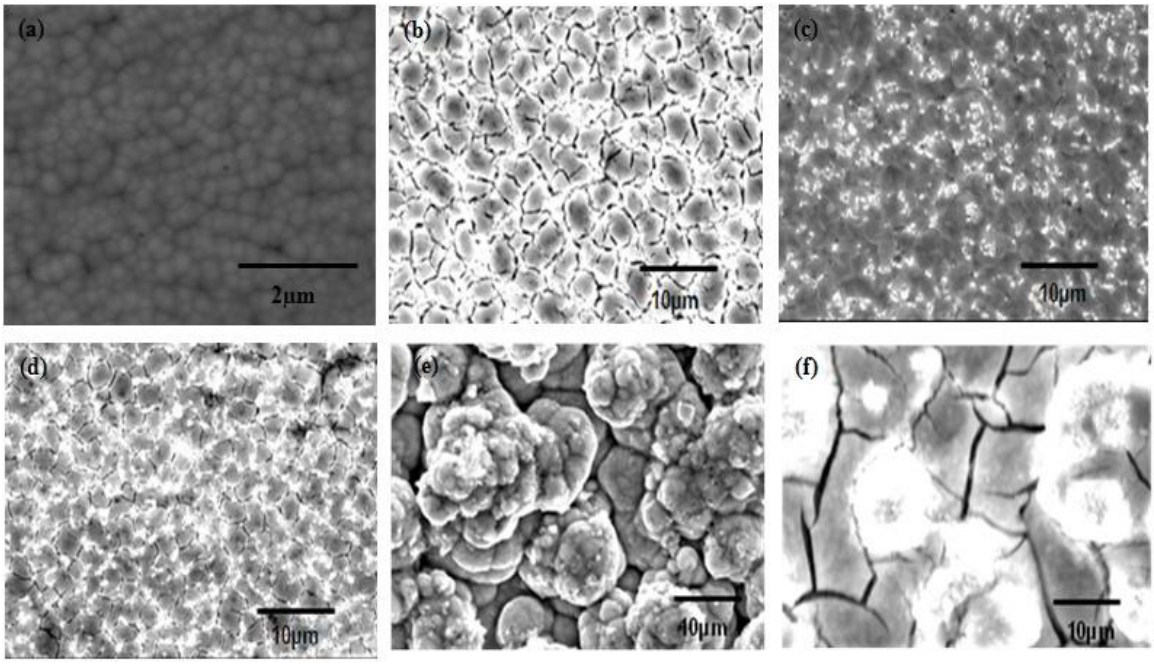

Fig. 4.14 *SEM images of the Co-W coating at (a) i=1A/dm^2; and Co-W composite coatings at (b) i=1A/dm^2, (c) i=3A/dm^2, (d) i=5A/dm^2, (e) i=7A/dm^2, (f) i=9A/dm^2 after etching.*

The grain boundaries are more clearly visible in crystalline samples after etching, giving a better idea of their grain structure. The surfaces of the coatings deposited at lower current densities ($\leq$ 5A/dm^2) showed distributed colonies of well defined granular features with alumina particles along the grain boundaries. The composite coatings show crystalline deposits till 5A/dm^2. Also, the grain size decreases with increasing current density till 5A/dm^2. At 1A/dm^2, the composite coating consisted of grains of various sizes ranging from 2.4-7.1 µm. At current densities of 3A/dm^2 and 5A/dm^2, the composite coatings consisted of grains in the size range of 1.5-3.5 µm and 1.3-2.8 µm respectively, thus, showing lesser variation in their sizes. The decrease in grain size can be attributed to the high overpotential gained by the increase in current

density. This overpotential increases the free energy of formation of nuclei leading to high nucleation rates and hence, smaller grains.

At 7A/dm^2, the surface is more nodular and consisted of coarse colonies of granular features unlike those observed at lower current densities as shown in Fig. 4.14 (e). The feature size in this coating ranges from 3-4.7 μm which is greater than that observed in the composite coatings at lower current densities (3 -5 A/dm^2). At 9A/dm^2, the coating is found to be cracking significantly and does not exhibit any well defined features. We can also observe the agglomeration of alumina particles at this parameter as shown in Fig. 4.14 (f). Thus, at higher current densities (7-9 A/dm^2), there is agglomeration of finer particles giving more random and coarser deposits.

The variation of grain size of composite coatings with current density is shown in Fig. 4.15. It clearly shows that finer deposits are obtained on increasing the current density till 5A/dm^2. On further increasing the current density, the grain size is found to increase significantly.

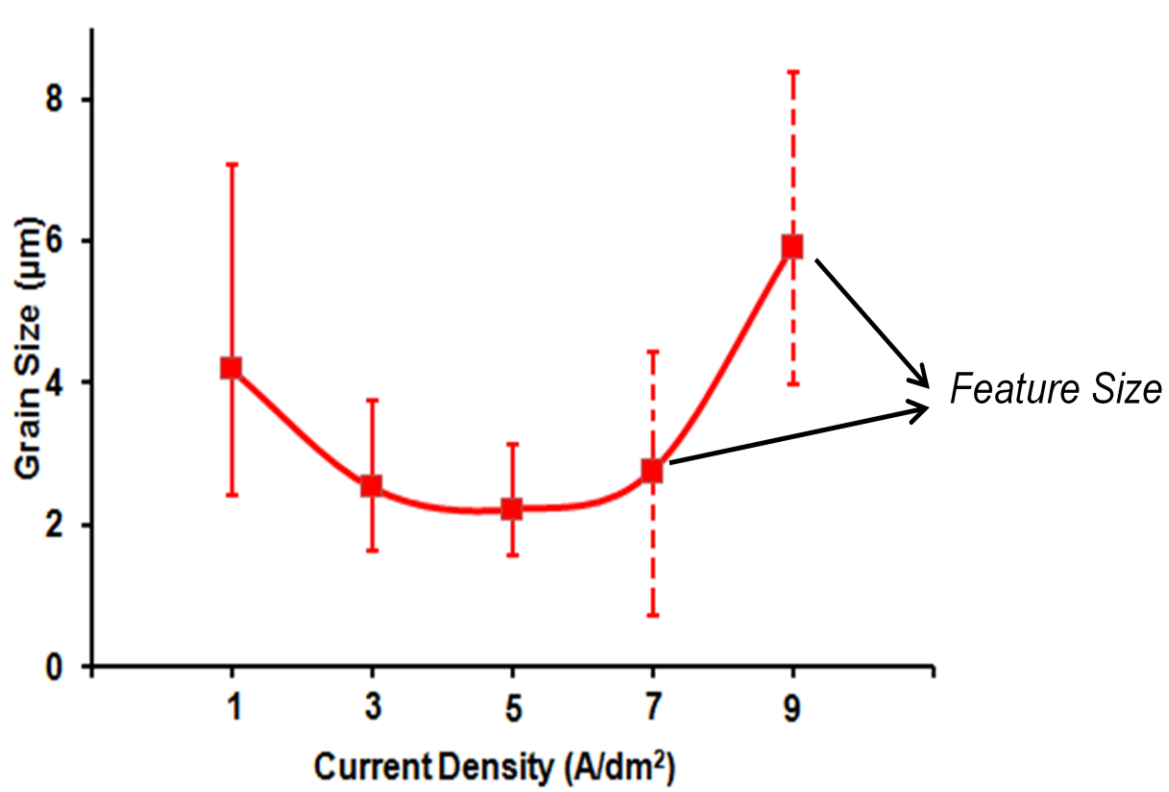

Fig. 4.15 *Variation of grain size with current density in composite coatings*.

The cross-sectional images of the composite coatings are presented in Fig. 4.16 (b-f). The average thickness of these coatings is found to the mostly constant with increasing current density and is found to in the range of 14µm to 16µm though the current density increases from 1A/dm^2 to 7A/dm^2 (Fig. 4.16 (d-e)). But, the thickness is found to be nearly 3 times (50-55µm approximately) for the composite deposited at 9A/dm^2 (Fig. 4.15 (f)). The deposit is non-uniform, and did not adhere well to the substrate; this might be due to high current density. Also, the coating thickness varied slightly across the sample surface and is found to be the greatest nearest to the centre of the sample. This is a direct consequence of the current distribution during deposition process [10].

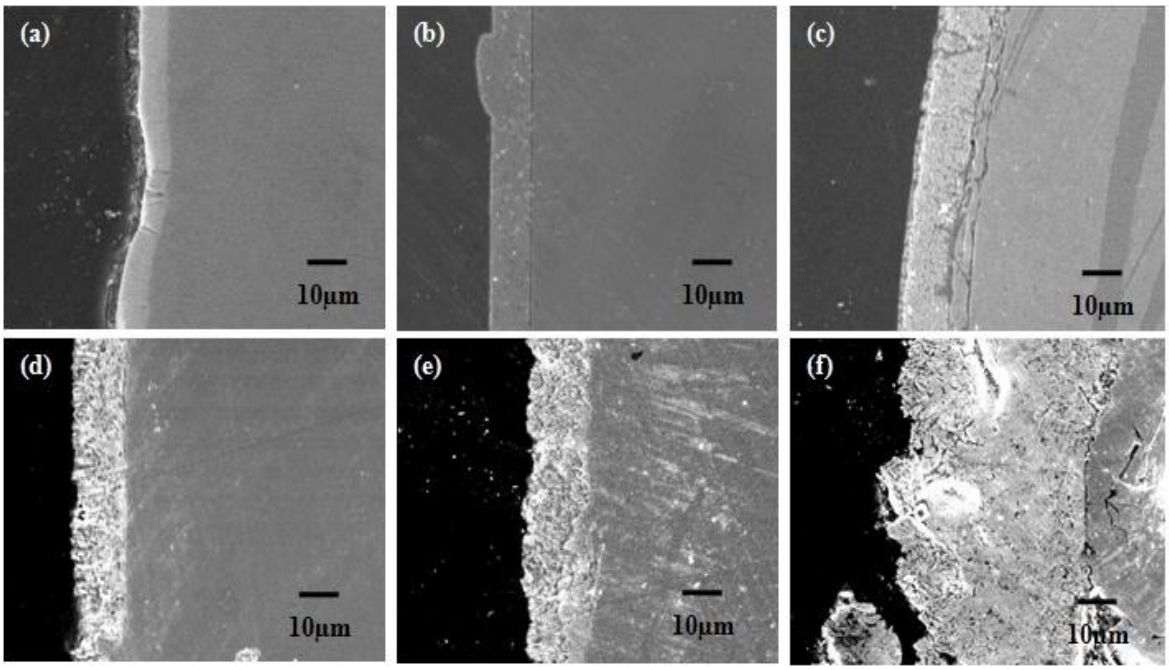

Fig. 4.16 *SEM images of the cross-section of Co-W coating at (a) i = 1A/dm^2; and Co-W composite coatings at (b) i = 1A/dm^2, (c) i = 3A/dm^2, (d) i = 5A/dm^2, (e) i = 7A/dm^2, and (f) i = 9A/dm^2.*

4.2.2 X-Ray Diffraction Analysis

Fig. 4.17 shows comparative XRD patterns of the composite coatings at different parameters in comparison with the Co-W coating. While Co-W coating exhibited amorphous nature as is evident from the broad halo between 42° ~ 46°, it is clear that the reinforcement of nano alumina into the deposit affected not only the nature of the thin film deposited, but also had an influence on its crystallographic orientation.

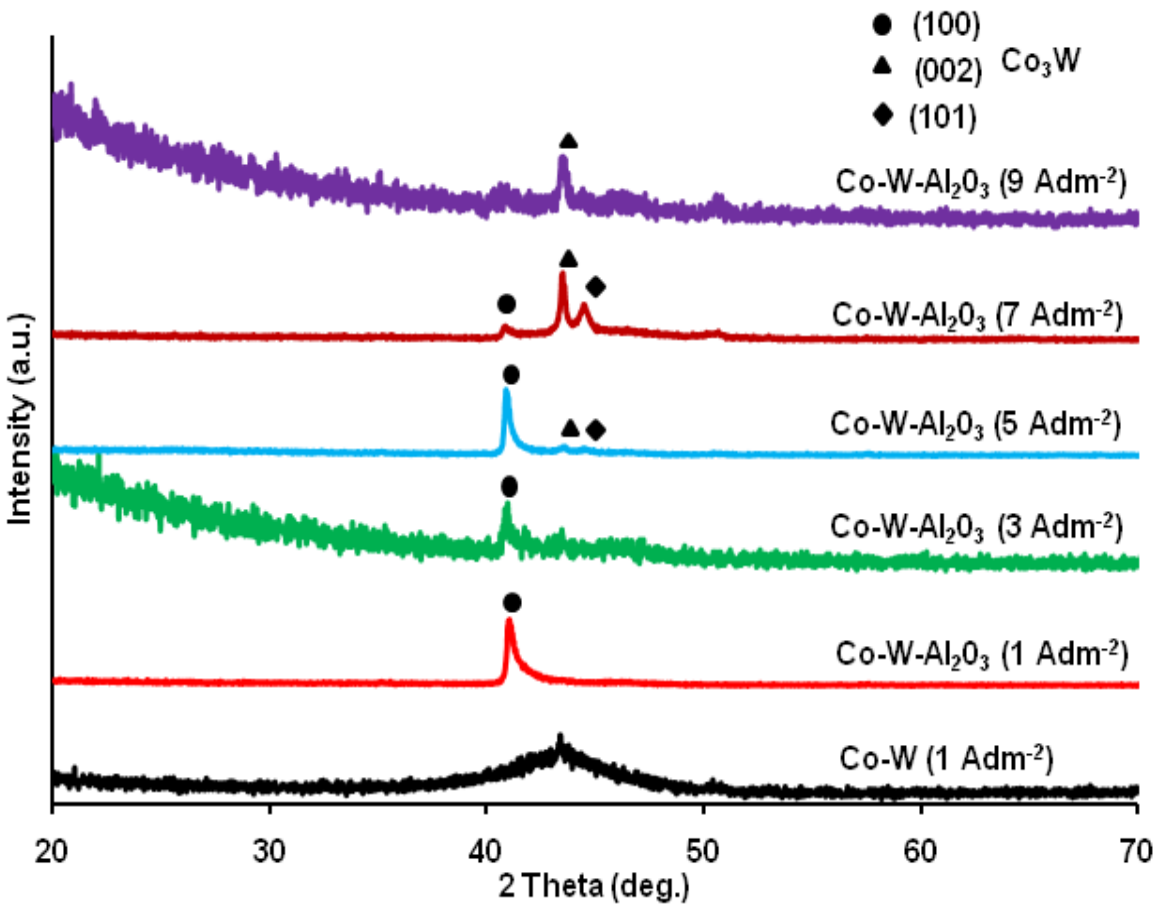

Fig. 4.17 *Comparision of X-Ray Diffraction Patterns of the coatings obtained at different current densities with that of Co-W coating.*

X-Ray diffraction analysis on the coatings produced at different current densities shows highly oriented crystals with sharp peaks for the composite coatings till 5A/dm^2. In these coatings, peaks are observed at 2θ values 41°, 44° and 47°, which correspond to (100), (002) and (101) orientations of the observed phase. They are indicative of the crystalline nature of the coatings which is also supported by the well defined grain structure of these composites. Those above 5A/dm^2 exhibited a broad halo with superimposed sharp peaks suggesting a mixed amorphous and crystalline nature of the coating. Phase analysis of the peaks shows the presence of Co_3W intermetallic phase near the peaks observed.

On keen examination of the XRD patterns, the composite coating at $1A/dm^2$ showed a strong peak of (100) plane. Diffraction peaks from (100) plane appear to increase with increasing current density and gradually (002) and (101) peaks also start to appear in the coating making it more crystalline in nature. The coating attains slight amorphous nature at $7A/dm^2$ and above, when a broad peak is observed along with other peaks of Co_3W. This might be an effect of increased particle reinforcement in the composite coating. Thus, the nature of the coating deposited changes due to the combined effect of the variation of process parameters and second phase particle reinforcement.

4.2.3 Compositional Analysis

Reinforcement of nano-alumina has been confirmed from the EDAX analysis which shows alumina content in the sample. The elemental composition of the coating at different current densities along with the microhardness of the coating has been presented in table 4.1. The table clearly shows the change in aluminum (i.e., alumina) and tungsten content with increasing current density.

Table 4.1: Table showing the atomic percentages of different elements in the composite coating at different current densities.

I (in A/dm^2)	Al, at %	W, at %	Co, at %	Microhardness (in HV)
1	10.44	13.05	74.18	720±20
3	12.47	8.51	62.67	807±20
5	20.1	9.77	52.25	885±20
7	16.48	7.94	47.17	604±20
9	76.58	6.18	13.12	534±20

Initially, it has been observed that the cobalt content of the coatings decreased as the alumina content increased. The tungsten content in the samples remained approximately constant here. Thus, it has been observed that increasing current density is promoting higher alumina reinforcement resulting in better properties of the coating until 5A/dm^2. Beyond this current density i.e., at 7A/dm^2, the co-deposited alumina has decreased along with a decrease in the tungsten and cobalt content. At relatively higher current densities above 7A/dm^2, decrease in cobalt and tungsten content in the coating is very prominent. But, at this parameter i.e., 9A/dm^2, the coating is cracking and there is agglomeration of alumina particles. This is also evident from the high aluminum content in the sample.

4.2.3 Microhardness

As compared to the Co-W coatings, the alumina reinforced samples are found to possess higher hardness values. While the hardness of the Co-W coating was found to be 600-650 HV (at similar parameters), the hardness of the reinforced samples varies from 700-920 HV. Fig 4.18 shows the

variation of microhardness of the coating with varying current density. Microhardness of the coating has increased with increasing current density until 5A/dm^2 and at higher current density the hardness was found to decrease significantly. The increase in hardness of the coating with current is attributed to the reinforced nano alumina particles and also varying cobalt and tungsten contents in the sample.

The microhardness of the coating increases with increasing reinforced nano-alumina particle content. The cobalt and tungsten content of the coating have their influence on the mechanical properties of the composite coatings. The alumina content is found to increase until 5A/dm^2 resulting in a corresponding increase in microhardness of the coating from 720 to 890 HV approximately. The coating at 7A/dm^2 exhibits lower hardness of the order of 600HV though the alumina content in the sample is higher. This is due to the significant decrease in the cobalt and tungsten content in the coating.

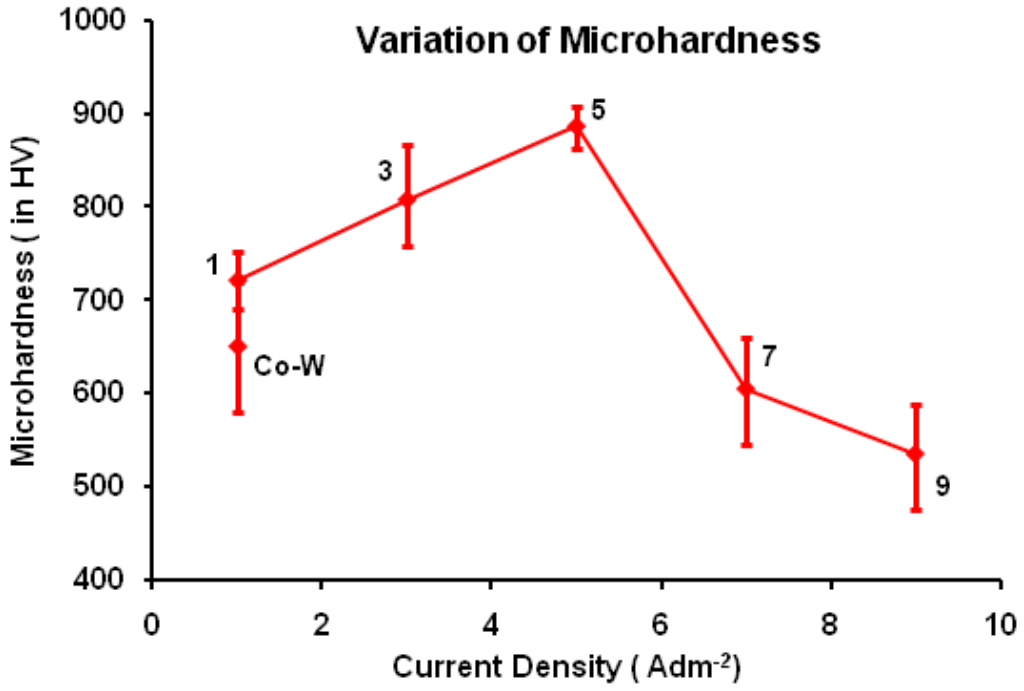

Fig. 4.18 *Graph showing variation of microhardness of the coating with current density.*

4.2.4 Wear Resistance

The resistance to sliding wear of as-deposited coatings was tested till 2400 cycles at specific load of 7N. The variation of coefficient of friction for all the composite coatings at dry sliding conditions against an alumina counterface during the first three minutes of operation is shown in Fig. 4.19.

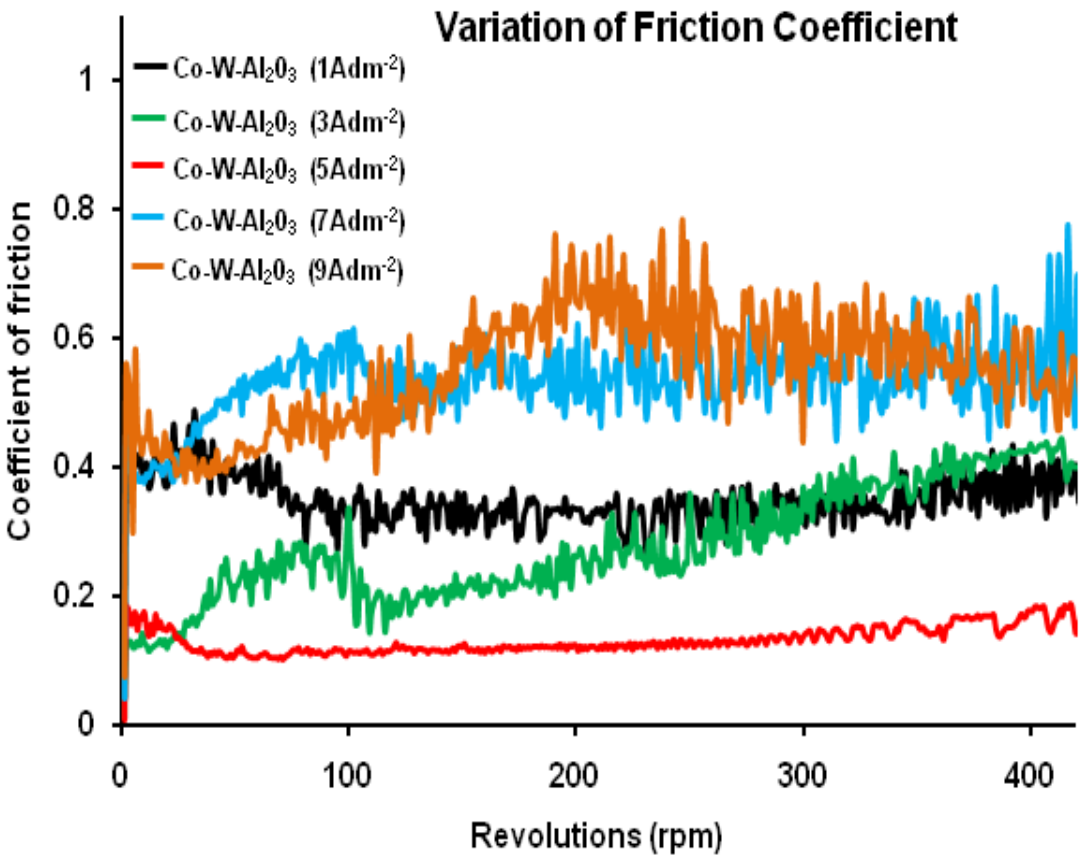

Fig. 4.19 *Variation of coefficient of friction of the composite coatings during ball-on-disc wear testing at load of 7N.*

The coefficient of friction exhibited by composite coatings deposited at varying current densities varied significantly. The average value of friction coefficient decreased from 0.314 at $1A/dm^2$ to 0.297 at $3A/dm^2$ and is found to be 0.138 for the coating deposited at $5A/dm^2$ (lowest among the composites deposited). The average value is again found to increase to 0.377 and then to 0.493 for the coatings deposited at 7 and $9A/dm^2$ respectively. The coefficient of friction is found to be lower than the Co-W coating (average friction coefficient is found to be nearly 0.465 for Co-W coating) for the composite coatings until $7A/dm^2$.

Fig. 4.20 shows weight loss in all the samples at the respective durations of the test. We can infer from the graph that the total weight loss is found to be decreasing with increasing current density until $5A/dm^2$ because of the higher alumina content and in turn higher hardness of the coating. So, higher alumina content, hardness and lower surface roughness resulted in higher wear resistance for obtained composite coatings until $5A/dm^2$. The average weight loss in these coatings during the total cycle of operation is found to decrease with increasing alumina content showing the improved wear resistance of the reinforced coatings.

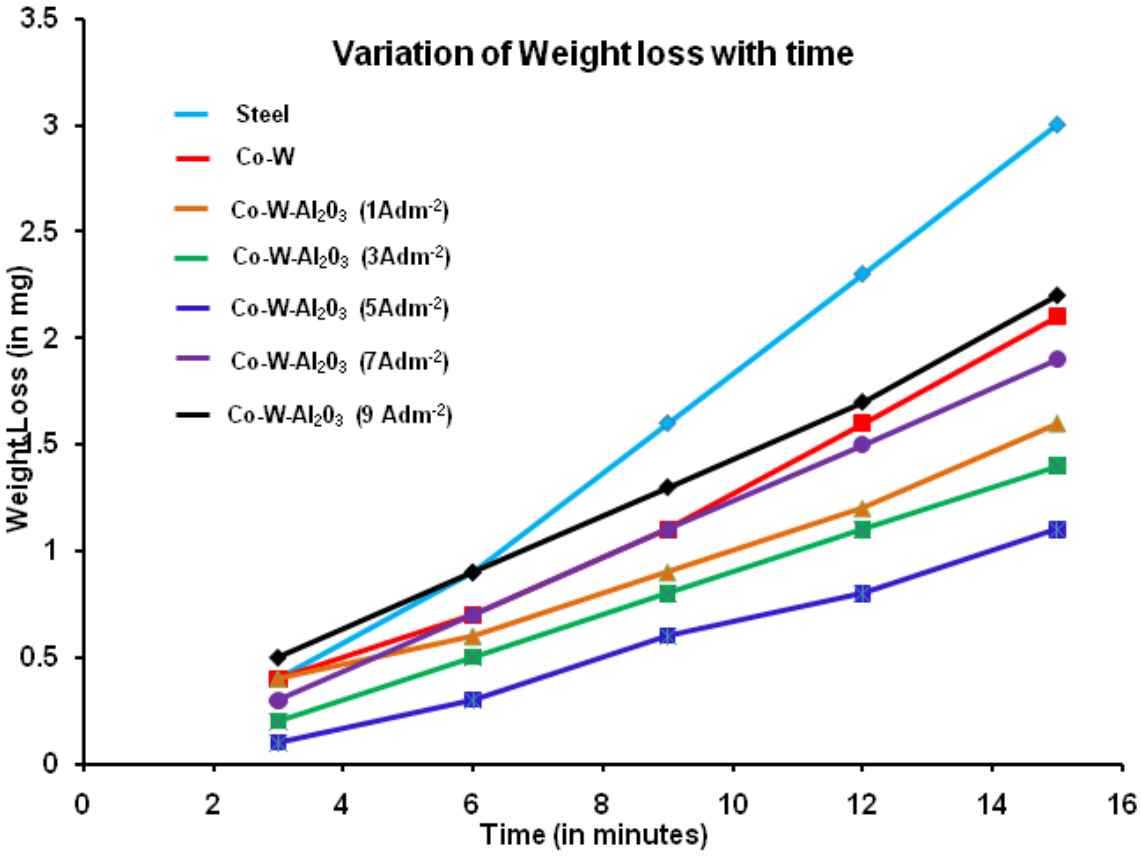

Fig. 4.20 *Graph showing variation of weight loss of the coatings and the substrate at different time intervals.*

The SEM images for the wear scars for all the composite coatings and the depth of the wear track in comparision to the wear scar of Co-W coating is shown in Fig. 4.21. They clearly show that the width and depth of the wear track decreases from the deposit at $1A/dm^2$ to $3A/dm^2$ and is found to be the least at $5A/dm^2$. It again increases for the coatings deposited at higher current densities (7 and $9A/dm^2$). This is in agreement with the values of the average friction coefficient value and weight loss in the coatings as observed above.

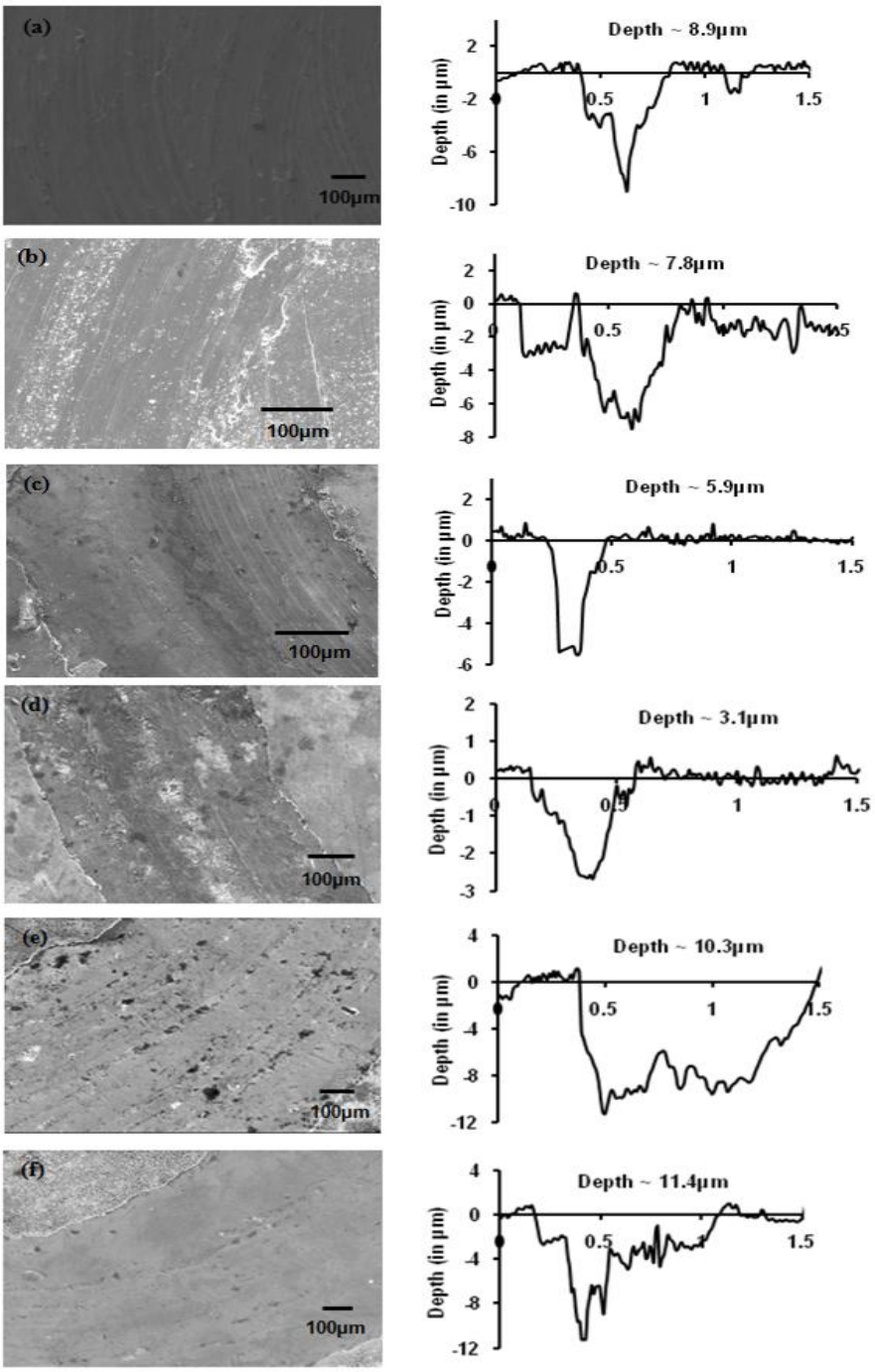

Fig. 4.21 *SEM images of the wear scar generated by ball on disc testing and the corresponding depth of the wear track generated (taken using profilometer) on the Co-W coating at (a) i=1A/dm^2; and the composite coatings at (b) i=1A/dm^2, (c) i=3A/dm^2, (d) i= 5A/dm^2, (e) i=7A/dm^2, (f) i=9A/dm^2.*

The above observations are further supported by finding the depth of the wear track for the composite coatings (in addition to the overall weight loss in the samples). Fig. 4.22 shows the variation of the overall weight loss of the composite coatings during wear testing with varying current density. The weight loss decreases with increasing current density because of the increasing alumina content, hardness and lower surface roughness until $5A/dm^2$. Above this value, the alumina content decreases accompanied by the decrease in cobalt and tungsten in the composite coating resulting in a decrease in wear performance of the coating at higher currents. The coating is also found to crack at very high current densities ($9A/dm^2$), resulting in increased weight loss and decreased wear resistance.

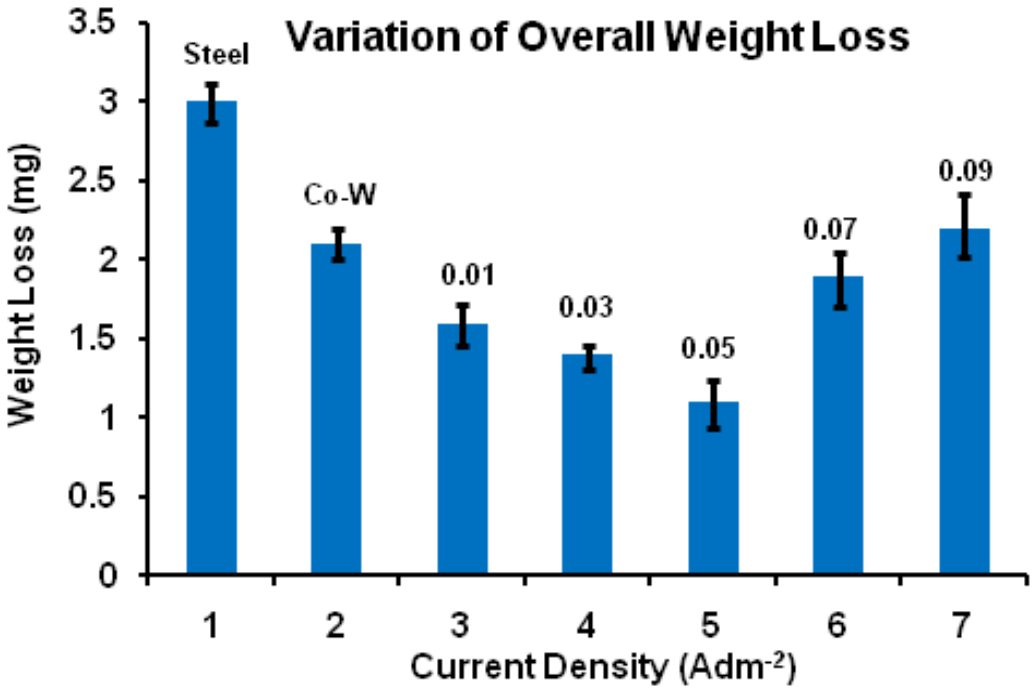

Fig. 4.22 *Overall graph showing the variation of weight loss in the coating with varying current density.*

Depth of the track is also found to vary in a similar manner as shown in Fig. 4.23. Thus, the sample deposited at current density of 5A/dm^2, 33% duty cycle and 333Hz frequency shows best properties namely, higher alumina content, hardness and wear resistance. Hence, these parameters are found to be the optimum parameters for the deposition process and also yield best properties for the composite coating as per our investigation.

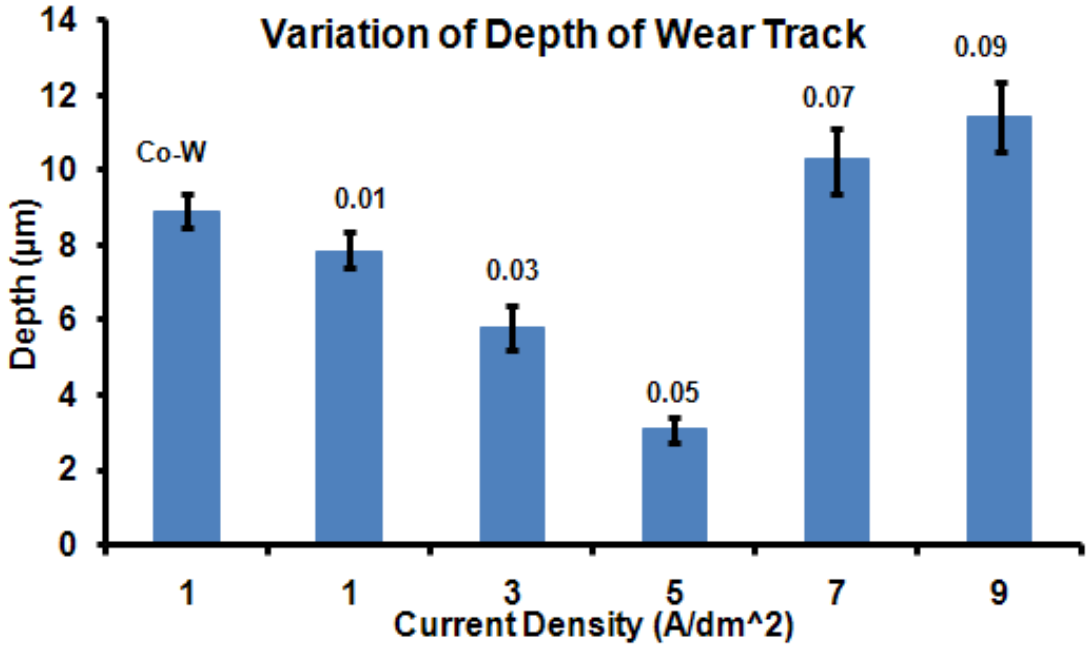

Fig. 4.23 *Bar Graph showing variation of depth of wear track with varying current density.*

The damage to the deposit is slight in comparision to the Co-W coated ones. On the other hand, the damage to the coating deposited at 5A/dm^2 is found to be the least among the composite coatings. It is also observed that there is some amount of chipping off of the material near the wear track for all the samples excepting for the coating deposited at 5A/dm^2 further confirming that this coating has improved wear resistance.

CHAPTER V

CONCLUSIONS

Synthesis of Co-W Coatings by Pulsed Electrodeposition as an Alternative to Hard Chrome Replacement

Pulsed electrodeposition (PED) of amorphous and crystalline Co-W coating using citrate bath is reported. The tendency to form amorphous coatings was found to be increased with increasing pulse duty cycle (at constant pulse frequency of 33 Hz) due to higher tungsten content (approaching intermetallic Co_3W composition). The crystalline to amorphous phase transitions in the coatings were also associated with changes in surface morphology from well-defined pyramidal grains to uniform refined grains. The surface microstructure, composition, phase, surface hardness, and roughness were found to be significantly influenced by PED processing parameters. The Co-W coatings with nanostructured surface features (150-200 nm) deposited with optimized pulse parameters (pulse duty cycle of 33.3 % and pulse frequency of 333 Hz) exhibited best hardness (575-725 HV). These coatings also showed significantly improved wear and corrosion resistance than stainless steel substrates.

Effect of Current Density on the Reinforcement of Al_2O_3 in Co-W Alloy Matrix and the Properties of Composite Coatings

Composite coatings of Co-W alloys with nano alumina are successfully fabricated using pulse electrodeposition process using citrate bath as electrolyte. Codeposition of alumina particles in the Co-W alloy matrix has enhanced the mechanical as well as tribological properties of the coating significantly. Crystalline and amorphous coatings have been deposited with hardness values in the range of 550-900 kg/mm^2 on variation of current density. The pin-on-disc wear testing data clearly demonstrated that the wear resistance of the composite coatings has improved considerably when compared with the Co-W coatings. This is attributed to the effect of high hardness, low surface roughness and alumina reinforcement in the composite coating. On investigation of the effect of current density on the dispersion of alumina particles into the alloy matrix and hence, the improvement of mechanical and tribological properties of the coating, it has been found that the coating deposited at $5A/dm^2$ exhibits best microhardness and possesses highest wear resistance among all the composite coatings. It exhibited hardness in the range of 850 to 900 kg/mm^2 comparable to that of Cr coatings.

CHAPTER VI

FUTURE WORK

- Detailed study on the tribological and corrosion behavior of Co-W coatings with variation of pulse parameters
- Analysis on glass forming ability of Co-W alloys with varying tungsten content
- Correlation of glass forming ability of Co-W alloys with their free energy of formation
- Effect of pulse parameters on the mechanical, tribological and corrosion characteristics of the composite coatings
- Detailed analysis of the corrosion behavior of composite coatings
- Studies on the effect of variation of alumina content on the mechanical, tribological and corrosion properties of the composite coatings

REFERENCES

[1] J. David Greenwood, *Hard Chromium Plating – A Handbook of modern practice*, 2nd Edition, Robert Draper Ltd, 1971.

[2] H. Royle, "Toxicity of chromic acid in the chromium plating industry (2)", *Environmental Research*, vol. 10, pp. 141-163, 1975.

[3] T. Norseth, "The carcinogenicity of chromium", *Environmental Health Perspectives*, vol. 40, pp. 121-130, 1981.

[4] S.D. Flora *et al.*, "Genotoxicity of chromium compounds – a review", *Mutation Research/Reviews in Genetic Toxicology*, vol. 338, pp. 99-172, 1990.

[5] F.W. Sunderman, "A review of the carcinogenicities of nickel, chromium and arsenic compounds in man and animals", *Preventive Medicine*, vol. 5, pp. 279-294, 1974.

[6] M. Bielewski, "Replacing cadmium and chromium", Institute for Aero Research, 2009.

[7] W. Xiaohe *et al.*, "Progress in developing electrodeposition for substitute hard chromium", *New Technology and New Process*, 2009.

[8] X. Wenying *et al.*, "Several new technologies to replace hard chromium plating", *Journal of Electroplating and finishing*, vol. 25, pp. 50-53, 2006.

[9] E.W. Brooman, "Wear behavior of environmentally acceptable alternatives to chromium coatings: cobalt based and other coatings", *Metal Finishing*, vol. 102, pp. 42-54, 2002.

[10] Z. Wanqiu, "Formation and Performance of Ni-W amorphous alloy deposit", *Journal of Electroplating and Finishing,* vol. 15, pp. 18-24, 1996.

[11] B. Muller *et al.,* "High temperature oxidation resistance of Ni-W coatings electroplated on steel, *Journal of Nanostructured Materials,* vol. 10, pp. 1285-1288, 1998.

[12] T. Yamasaki *et al.,* "Formation of ductile - amorphous and nanocrystalline Ni-W alloys by electrodeposition", *Journal of Plating and Surface Finishing,* vol. 87, pp. 148-152, 2000.

[13] W.U. Gang *et al.,* "The microstructure and hardness of electrodeposited Co-Ni alloy coatings", *Journal of Materials Science and Tehnology,* vol 10, pp. 419-423, 2002.

[14] N.E. Fenineche *et al.,* "Structure and magnetic properties of nanocrystalline Co-Ni and Co-Fe mechanically alloyed", *Materials Letters,* pp. 4493-4497, 2003.

[15] Z.L. Qun *et al.,* "Alternatives to chromium plating – Ni-W and Ni-W-B amorphous alloy deposits", *Journal of Electroplating and Finishing,* vol. 23, pp. 10-16, 2004.

[16] J. Shuguo *et al.,* "Investigation on electrodeposit technology of Ni-W-P amorphous alloy", *Journal of Physics,* pp. 19-23, 1999.

[17] H.J. Yun *et al.,* "Characterisation of electrodeposited Co-W-P amorphous coatings on carbon steel", *Electroceimca Acta,* vol. 54, pp. 370-375, 2008.

[18] H.E. Fengjiao *et al.,* "Friction and wear behavior of electrodeposited amorphous Fe-Co-W alloy deposits", *The Transcations of Nonferrous Metals Society of China,* vol. 14, pp. 901-906, 2004.

[19] M. Srivastava *et al.,* "Structure and properties of electrodeposited Ni-Co-YZA composite coatings, *Journal of Applied Electrochemistry,* vol. 38, pp. 669-677, 2008.

[20] C.P. Steffani *et al.,* "Electrodeposition and corrosion resistance of Ni-W-B coatings", *Journal of Materials and Engineering Performance,* vol. 6, pp. 413-416, 1997.

[21] Z.Ping *et al.,* "Ni-P-SiC composite coatings electroplating on carbon steel assisted by mechanical attrition", *Acta Materials,* vol. 23, pp. 1-10, 2010.

[22] Z.Guo *et al.,* "Studies on the wear resistance and structure of electrodeposited RE-Ni-W-P-SiC-PTFE composite materials, *Surface and Coatings Tehnology,* vol. 181, pp. 141-145, 2004.

[23] K.H. Hou *et al.,* "Preparation and wear resistance of pulse electrodeposited Ni-W/Al_2O_3 composite coatings", *Applied Surface Science,* vol. 257, pp. 6130-6136, 2011.

[24] B.S.B. Reddy *et al.,* "Pulsed co-electrodeposition and characterization of Ni-based nanocomposites reinforced with combustion-synthesized, undoped, tetragonal-ZrO_2 particulates", *Nanotechnology,* vol. 19, pp. 115603-115613, 2008.

[25] V.Y. Dolmatov *et al.,* "Preparation of wear-resistant chromium coatings using different types of nanodiamonds", *Powder Metallurgy and Metal Ceramics,* vol. 42, pp. 587-591, 2003.

[26] G.Heidari *et al.,* "Nano SiC-Nickel composite coatings from a sulfamat bath using direct current and pulsed direct current", *Journal of Materials Engineering and Performance,* vol. 19, pp. 1193-1198, 2010.

[27] A.F. Zimmerman *et al.,* "Pulse electrodeposition of Ni-SiC nanocomposite", *Materials Letters,* vol. 52, pp. 85-90, 2002.

[28] X.J. Sun and J.G. Li, "Friction and wear properties of electrodeposited nickel-titania nanocomposite coatings", *Tribology Letters,* vol. 28, pp. 223-228, 2007.

[29] H. Gul *et al.,* "Characteristics of electro-co-deposited Ni- Al_2O_3 nano-particle reinforced metal matrix composite (MMC) coatings", *Wear*, vol. 267, pp. 976-990, 2009.

[30] P. Papavasilopoulou *et al.,* "Effect of plating parameters on NiP-SiC electrodeposition", *Proceeding of the 7th International Conference – The Coatings in Manufacturing Engineering*, pp. 417-425, 2008.

[31] U. Erb *et al.,* "Nanostructured Materials-Processing, Properties and Potential Applications", William Andrew Publishing, 2002.

[32] I. Gurrappa, and L. Binder, "Electrodeposition of nanostructured coatings and their characterization - a review", *Science and Technology of Advanced Materials*, vol. 9, pp. 1-11, 2008.

[33] A. Krohn and C.W. Bohn, **"**Electrodeposition of alloys: Present state of the art", *Electrodeposition and Surface Treatment*, vol. 1, pp. 199-211, 1973.

[34] N. Kanani, *Electroplating – Basic Principles, Processes, and Practice*, Elsevier Advanced Technology, 2004.

[35] M.S. Chandrasekar and P. Malathy, "Pulse and pulse reverse plating—Conceptual, advantages and applications", *Electrochimica Acta*, vol. 53, pp. 3313–3322, 2008.

[36] A.G. Gray, *Modern Electroplating*, John Wiley & Sons, 1953.

[37] G. Devaraj *et al.*, "Pulse Plating- Review", *Material Chemistry and Physics*, vol. 25, pp. 439-461, 1990.

[38] A. Brenner, *Electrodeposition of Alloys – Principles and Practice*, Volume 1, Academic Press Inc., 1963.

[39] T. Borkar and Sandip Harimkar, "Microstructure and Wear Behavior of Pulse Electrodeposited Nickel-Carbon Nanotube (Ni-CNT) Composite Coatings," *Surface Engineering,* vol. 2010.

[40] T. Watanabe, *Nano-Plating – Microstructure Control Theory of Plated Film and Database of Plated Film Microstructure*, Elsevier Ltd., 2004.

[41] T. Borkar and Sandip Harimkar, "Effect of electrodeposition conditions and reinforcement content on microstructure and tribological properties of nickel composite coatings", *Surface and Coatings Technology*, vol. 205, pp. 4124-4134, 2011.

[42] P.N. Branko, "Electrodeposition of alloys and composites with superior corrosion and electrocatalytic properties", *Plating and surface finishing A.*, vol. 91, pp. 40-49, 2004.

[43] F. H. Froes *et al.,* "Synthesis of nanocrystalline materials - an overview", *Materials Science and Engineering A*, vol. 301, pp. 44-53, 2001.

[44] P.L. Cavallotti *et al.,* "Phase Structure of electrodeposited alloys", *Electrochemica Acta*, vol. 50, pp. 4557-4565, 2005.

[45] M. Musiani, "Electrodeposition of composites: an expanding subject in electrochemical materials science", *Electrochimica Acta*, vol. 45, pp. 3397–3402, 2000.

[46] C.T.J. Low *et al.*, "Electrodeposition of composite coatings containing nanoparticles in a metal deposit", *Surface & Coatings Technology*, vol. 201, pp. 371–383, 2006.

[47] L. Benea *et al.*, "Composite Electrodeposition to obtain nanostructured coatings", *Journal of The Electrochemical Society*, vol. 148, pp. C461-C465, 2001.

[48] N. Guglielmi, "Kinetics of the deposition of inert particles from electrolytic baths", *Journal of Electrochemical Society*, vol. 119, pp. 1009-1012, 1972.

[49] A.M.J. Kariapper and J. Foster, "Further studies on the mechanism of formation of electrodeposited composite coatings", *Transactions of the Institute of Metal Finishing*, vol. 52, pp. 87-91, 1974.

[50] J.P. Celis and J.R. Roos, "Kinetics of the deposition of alumina particles from copper sulfate plating baths", *Journal of the Electrochemical Society*, vol. 124, pp. 1508-1511, 1977.

[51] J.P. Celis *et al.*, "A mathematical model for the electrolytic codeposition of particles with a Metal Matrix", *Journal of the Electrochemical Society*, vol. 134, pp. 1402-1408, 1987.

[52] V.V. Rudneva and G.V. Galeskii, "Electrodeposition and properties of composite coatings with nanocomponents", *Steel in Translation*, vol. 37, pp. 224-228, 2007.

[53] T. Watanabe, "Current topics in amorphous materials: physics and technology", *Elsevier Publishers*, pp. 139-149, 1993.

[54] W. Betteridge, *Cobalt and its alloys*, John Wiley & Sons, 1982.

[55] J.R. Davis, *Nickel, Cobalt and Their Alloys*, ASM Speciality Handbook, ASM International, 2000.

[56] R. Breckpot *et al.*, *Cobalt Monograph*, Cobalt Development Institute, 1960.

[57] R.A. Prado, "Electrodeposition of nanocrystalline cobalt alloys coatings as a hard chrome alternative, 2009 DoD Corrosion Conference, 2009.

[58] W. Pattsch, "Pulsed electrodeposition of zinc and cadmium*", Theory and Practice of Pulse Plating*, pp. 93-99, 1986.

[59] J. Cl. Puippe, "Influence of charge and discharge of electrical double layer in pulse plating, *Theory and Practice of Pulse Plating*, pp. 41-53, 1986.

[60] M.R.M. Krishnappa *et al.,* "Effects of current density on electrodeposited CoMnP thin films", *Journal of Engineering and Applied Sciences,* vol. 5, pp. 6-10, 2010.

[61] A.M. Rashidi and A. Amadeh, "Effect of electroplating parameters on microstructure of nanocrystalline nickel coatings", *Journal of Materials Science and Tennology,* vol. 26, pp.82-86, 2010.

[62] D. I. Rehrig *et al., Plating and Surface Finishing*, vol. 64, pp. 40-44, 1977.

[63] C. Shanti *et al.,* "The effect of pulse paramaters in electrodeposition of silver alloy", *Materials Letters,* vol. 62, pp. 4519-4521, 2008.

[64] K.M. Youssef *et al.,* "Influence of pulse plating parameters on the synthesis and preferred orientation of nanocrystalline zinc from zinc sulfate electrolytes", *Electrochemica Acta,* vol. 54, pp. 677-683, 2008.

[65] K.M. Youssef, "Influence of additives and pulse electrodeposition parameters on production of nanocrystalline zinc from zinc chloride electrolytes", *Journal of Electrochemical Society,* vol. 151, pp. C103-C111, 2004.

[66] V. Thangaraj *et al.,* "Development of Zn-Co alloy coatings by pulsed current from chloride bath", *Indian Journal of Chemical Technology,* vol. 15, pp. 581-587, 2008.

[67] P. Ganesan *et al.,* "Development of Zn-Ni-Cd coatings by pulse electrodeposition process", *Surface and Coatings Technology,* vol. 201, pp. 3658-3669, 2006.

[68] S. Yoshimura *et al.,* "Pulsed current electrodeposition of palladium", *Metal Finishing,* vol. 81, pp. 39-42, 1986.

[69] K.P. Gupta, "The Co-Cr-W (cobalt-chromium-tungsten) system", *Journal of Phase Equilibria and Diffusion,* vol. 27, pp. 178-183, 2006.

[70] V.V. Shtefan *et al.*, "Regularities of the deposition of cobalt-tungsten alloys by pulsed currents", *Materials Science*, vol. 43, pp. 429-433, 2007.

[71] H. Capel *et al.*, "Sliding wear behavior of electrodeposited cobalt-tungsten and cobalt-tungsten-ion alloys, *Wear*, vol. 225, pp. 917–923, 2003.

[72] Z.A. Hamid, "Electrodeposition of cobalt–tungsten alloys from acidic bath containing cationic surfactants", *Materials Letters*, vol. 57, pp. 2558–2564, 2003.

[73] M.A. Ibrahim *et al.*, "Electrodeposition of nanocrystalline cobalt-tungsten alloys from citrate electrolyte, *Journal of Applied Electrochemistry*, vol. 33, pp. 627–633, 2003.

[74] G.Z. Grabco *et al.*, "Micromechanical Properties of Co-W Alloys Electrodeposited under Pulse Conditions", *Surface Engineering and Applied Electrochemistry*, vol. 43, pp. 11–17, 2007.

[75] H. Cesiulis *et al.*, "Electrodeposition of Co-W Alloys with P and Ni", *Materials Science, vol.* 15, pp. 115-122, 2009.

[76] F. Chraibi *et al.*, "Influence of Citrate Ions as Complexing Agent for Electrodeposition of $CuInSe_2$ Thin Films", *Physica Status Solidi (a)*, vol. 186, pp. 373 – 381, 2001.

[77] M. Ved *et al.*, "Structure and Properties of electrolytic cobalt-tungsten alloy coatings", *Functional materials*, vol. 15, pp. 613-616, 2008.

[78] L.P. Wang *et al.*, "A comparative study on the tribological behavior of nanocrystalline nickel and cobalt coatings correlated with grain size and phase structure"**,** *Materials Chemistry and Physics*, vol. 99, pp. 96-103, 2006.

[79] N. Tsyntsaru *et al.*, "Tribological And Corrosive Characteristics of Electrochemical Coatings Based On Cobalt And Iron Superalloys", *Powder Metallurgy and Metal Ceramics*, vol. 48, pp. 419-428, 2009.

[80] N.Tsyntsaru *et al.*, "Iron-tungsten alloys electrodeposited under direct current from citrate-ammonia plating baths", *Surface and Coatings Technology*, vol. 203, pp. 3136-3141, 2009.

[81] D.P. Weston *et al.*, "Nanostructured Co-W coatings produced by electrodeposition to replace hard Cr on aerospace components", *Transactions of the Institute of Metal Finishing*, vol. 88, pp. 47-56, 2010.

[82] S.A. Silkin *et al.*, "Electrodeposition of Nanocrystalline Co-W Coatings from Citrate Electrolytes Controlled Hydrodynamic Conditions, Part 3: The Micro_ and Macrodistribution of the Deposition Rates, the Structure, and the Mechanical Properties", *Surface Engineering and Applied Electrochemistry*, vol. 46, pp. 206–214, 2010.

[83] C.L. Aravinda *et al.*, "Electrodeposition and deposition of Co-W alloy films", *Journal of Applied Electrochemistry*, vol. 30, pp. 601-606, 2000.

[84] T. Toda, "On the temper hardening properties of cobalt tungsten alloys", *Materials Transactions*, vol. 6, pp. 139-146, 1965.

[85] J. Dutkiewicz and G. Kostorz, "Strengthening of cobalt tungsten alloys upon discontinuous precipitation", *Acta Materials*, vol. 38, pp. 2283-2286, 1990.

APPPENDIX – I

Below mentioned papers are based on the work presented in this thesis and are submitted to journals recently

- **Mrinalini Mulukutla**, Vamsi Karthik Kommineni, Sandip P. Harimkar, Pulsed Electrodeposition of Co-W Amorphous/Nano-Crystalline Coatings, *Applied Surface Science* (In Review).
- **Mrinalini Mulukutla**, Sandip P. Harimkar, Surface Properties Measurement, *Engineering Measurements Encyclopedia*, Wiley Publishers (In Press).
- **Mrinalini Mulukutla**, Sandip P. Harimkar, Electrodeposition of Co-W-Al_2O_3 Composite Coatings for Hard Chrome Replacements, *Journal of Materials Engineering and Performance* (In Review).

VITA

Siva Prashanta Mrinalini Mulukutla

Candidate for the Degree of

Master of Science

Thesis: PULSE ELECTRODEPOSITION OF Co-W AND ITS COMPOSITE COATINGS FOR HARD CHROME REPLACEMENTS

Major Field: Mechanical and Aerospace Engineering

Biographical:

Education:

Completed the requirements for the Master of Science in mechanical engineering at Oklahoma State University, Stillwater, Oklahoma in July, 2011.

Completed the requirements for the Bachelor of Engineering in your Metallurgical Engineering at Andhra University, Visakhapatnam, Andhra Pradesh, INDIA in 2008.

Experience:
Has over 3years of experience in research related fields and worked on fabrication and characterization of materials processed by advanced processing routes.

Professional Memberships: IIM, TMS, AcerS, ASM, AIST.

Name: Siva Prashanta Mrinalini Mulukutla Date of Degree: July, 2011

Institution: Oklahoma State University Location: Stillwater, Oklahoma

Title of Study: PULSE ELECTRODEPOSITION OF Co-W AND ITS COMPOSITE COATINGS FOR HARD CHROME REPLACEMENTS

Pages in Study: 87 Candidate for the Degree of Master of Science

Major Field: Mechanical and Aerospace Engineering

Replacement of hard chromium plating has been of particular interest to many industrial applications, including automotive, aircraft, and machinery parts that require high hardness and wear/corrosion resistance. Electrodeposition is chosen as it is one of the most common, relatively simple, and economical coating technologies capable of depositing metal and alloy coatings with improved surface properties and microstructures. Efforts are directed towards electrodeposition of an amorphous alloy/composite coatings that present the potential for replacing conventional hard chrome coatongs.

Co-W alloy coatings, owing to their eco-friendly processing and high hardness/wear resistance, are promising for electrolytic chromium replacement. In this study, pulsed electrodeposition of amorphous and crystalline Co-W coatings is performed. Systematic investigations on the effect of pulse duty cycle and pulse frequency on development of surface microstructure, phases, composition, surface roughness, and micro-hardness are conducted to optimize the parameters of the deposition process. Furthermore, an attempt is made to fabricate composite coatings of Co-W alloys with nano alumina particles as reinforcement. Codeposition of alumina particles in the Co-W alloy matrix has enhanced the mechanical as well as tribological properties of the coating significantly.

ADVISER'S APPROVAL: Dr. Sandip P. Harimkar